Facility Response RAI SAR 4.1 items (a) and (b):
The methods used to adequately model and characterize the physics behavior of the UMLRR have been documented in many internal reports and conference papers over the last 25+ years. The physics modeling efforts have primarily utilized the SCALE package for cross section generation and the VENTURE diffusion theory code for obtaining the power and few-group flux distributions within the UMLRR, and for most routine reactivity evaluations involving blade worth distributions, excess reactivity evaluations, etc.. In addition, in 2012, a detailed MCNP model of the UMLLR was constructed and, since that time, the MCNP model has been used, as needed, to validate and expand upon our VENTURE UMLRR modeling capability and to support specific studies where few-group diffusion theory is clearly inappropriate (prior to the development of the MCNP model, the DORT transport theory code was utilized for studies where diffusion theory was not adequate).

Overall, the combined use of the VENTURE and MCNP models (and earlier DORT models) give a reasonable representation of the physics behavior of the UMLRR, and ample evidence has been accumulated over the years that support confidence in these tools. Two successful modeling efforts, in particular, which involved the HEU to LEU design and conversion effort (which was completed in 2000) and the design, implementation, and testing of an excore fast neutron irradiator (which was completed in 2002), have been documented in some detail (see Refs. 1-4, for example). These confirm the adequacy of our past modeling capabilities.

More recently in 2011-2012, in support of the Worcester Polytechnic Institute (WPI) fuel transfer study, the 3-D VENTURE models were improved and updated to allow both the standard UMass-Lowell U_3Si_2-Al fuel elements and the UAl_x-Al WPI fuel elements to fit within the same model. As part of that effort, in conjunction with the development of the MCNP model that was occurring at the same time, some further benchmarking of the new models was completed and Refs. 5-7, in particular, provide sufficient detail concerning both the 3-D VENTURE and MCNP models, along with several inter-comparisons and evaluations relative to actual measured data for the UMLRR. In most cases, the results are quite satisfactory and support the use of these computational models to generate much of the physics data used within the current UMLRR SAR.

To be explicit, Tables 1 and 2 and Fig. 3 from Ref. 6 have been extracted and included here to show some VENTURE and MCNP results for a few different UMLRR core configurations. A detailed discussion of these results is given in the full reports but, as apparent from just a quick review, the models seem to do a reasonable job at predicting the base eigenvalues (with about a negative 2 - 2.5% bias for the VENTURE results), the proper blade worth distributions, and several axial flux profiles in the initial LEU startup core (M-1-3 configuration). The comparisons are reasonable considering the uncertainty inherent in the measured data (especially for the measured blade worths). The model predictions have been sufficient for routine design and analysis purposes and for preparing data for the safety analyses reported upon in the Oct. 2015 UMLRR SAR.

In addition, although depletion effects have not been significant for the UMLRR (due to relatively low cumulative burnup of the LEU fuel since 2000), the updated set of figures provided below (with originals from Ref. 7), show that the VENTURE depletion model provides a reasonable treatment of the fuel depletion and fission product buildup within the reactor.

In summary, the data presented here (and in more detail in the complete reports in Refs. 5 - 7) establish existing local capability to adequately model the physics characteristics of the UMLRR. These same tools (primarily the SCALE + VENTURE combination) have been used to determine most of the reference parameters for the safety analyses within the SAR (excess reactivity, blade worths, shutdown margin, peaking factors, etc.) and, along with reasonable margins, the values used provide a reasonable representation of actual expected UMLRR behavior.

The following tables (Tables 1 & 2) and figure (Fig. 3) are directly from Ref. 6

Table 1 Summary results for several critical configurations within the UMLRR.

Model Description	Blades 1-4 Location (inches out)	Regulating Blade Location (inches out)	VENTURE K_{eff}	MCNP K_{eff}
BOL M-1-3	15.3	8.0	0.980	0.995
BOL M-2-5	14.9	10.0	0.978	0.999
M-2-5 at 50 MWD	16.3	7.7	0.975	0.996

Table 2 Computed vs. measured blade worths for three UMLRR configurations.

	M-1-3 BOL Core Total Worth (% Δk/k)			M-2-5 BOL Core Total Worth (% Δk/k)			M-2-5 at 50 MWD Total Worth (% Δk/k)		
Blade #	**Expt.**	**VENT**	**MCNP**	**Expt.**	**VENT**	**MCNP**	**Expt.**	**VENT**	**MCNP**
Blade 1	2.63	2.95	3.00	2.82	2.91	2.76	2.55	2.86	2.73
Blade 2	2.47	2.80	2.75	2.19	2.35	2.40	2.23	2.29	2.40
Blade 3	3.32	3.32	3.42	3.19	3.16	3.42	3.64	3.06	3.19
Blade 4	3.20	3.43	3.55	3.93	3.72	3.83	4.19	3.74	3.71
Total Blades 1–4	11.6	12.5	12.7	12.1	12.1	12.4	12.6	12.0	12.1
Excess K_{eff} Blades 1–4	2.82	3.22	3.44	3.46	3.45	3.46	2.41	2.71	2.60
Regulating Blade	0.28	0.44	0.38	0.30	0.45	0.38	0.31	0.45	0.38

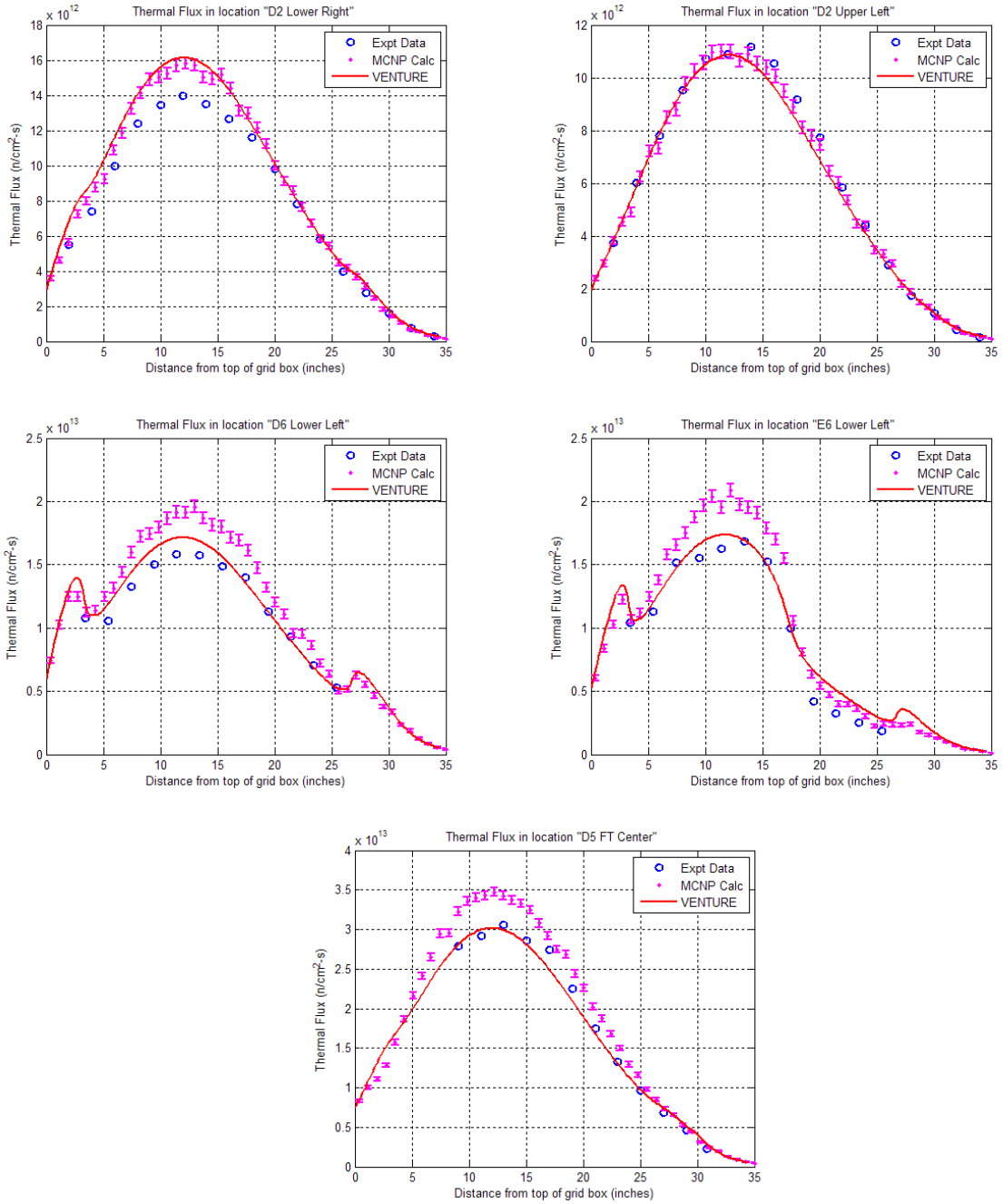

Fig. 3 Calculated vs. measured axial thermal flux profiles at various locations (M-1-3).

Updated results (from June 2015) for Figs. 3, 4, 16, and 17, respectively from Ref. 7

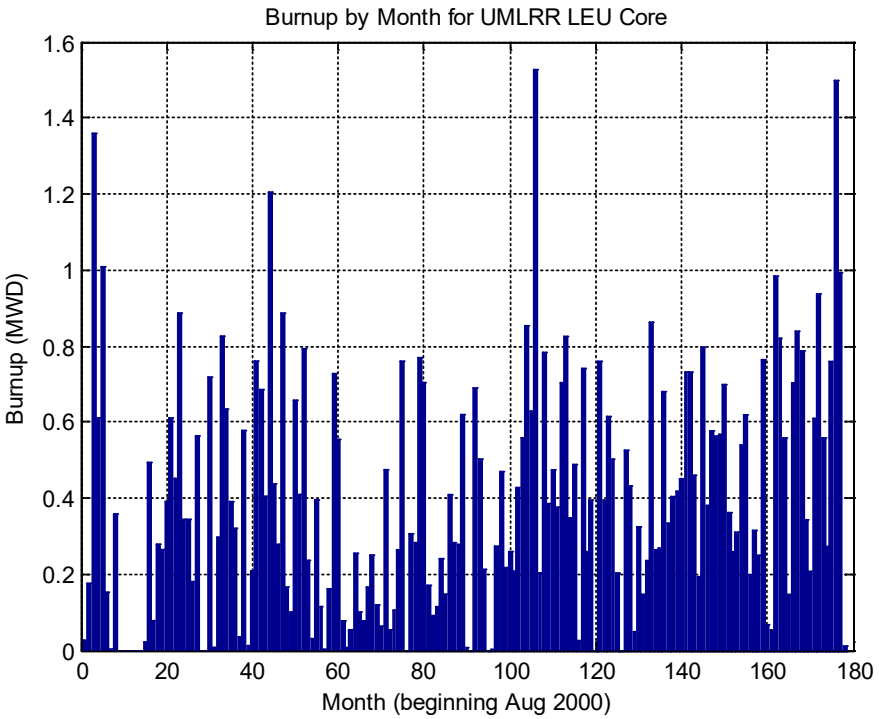

Fig. 3 Burnup rate history for the UMLRR LEU core.

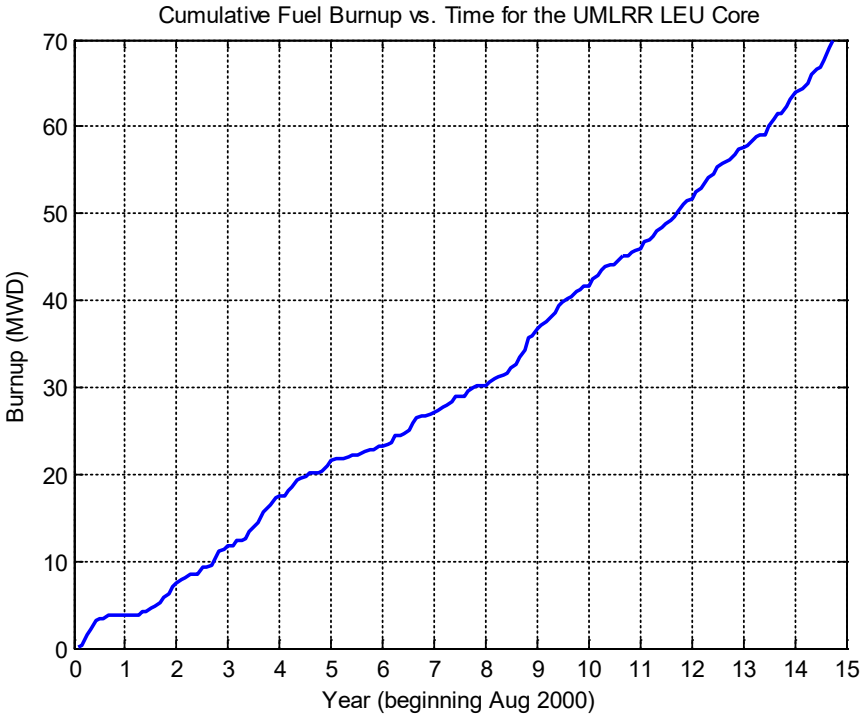

Fig. 4 Cumulative burnup history for the UMLRR LEU core.

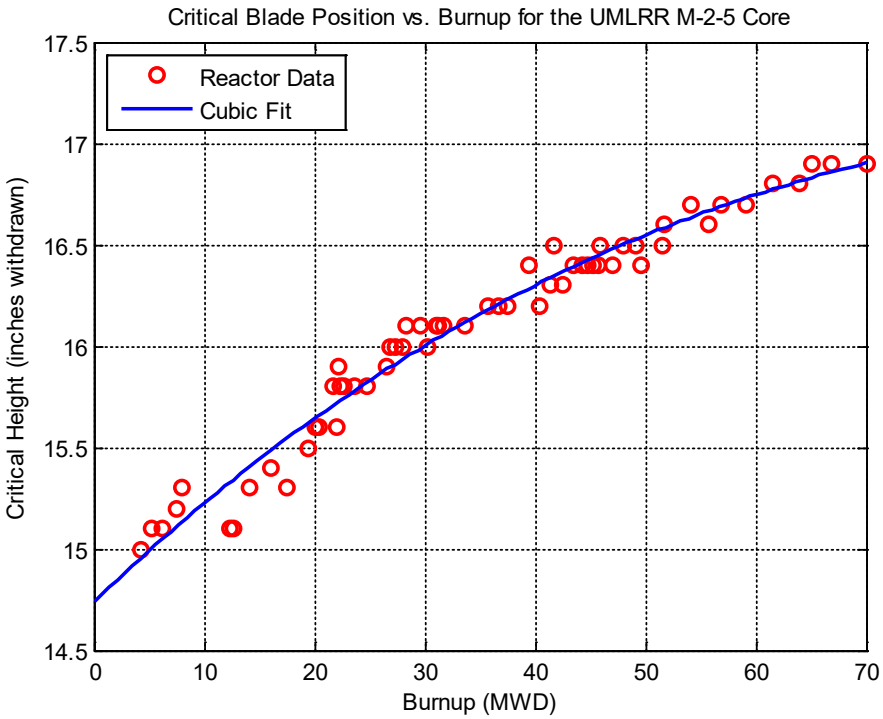

Fig. 16 Critical blade height vs. burnup for the UMLRR M-2-5 core.

Note: Much of the variability that is apparent in the raw data is due to a changing regulating blade position and differing pool temperatures. The data were collected on days when the residual Xe reactivity was negligible.

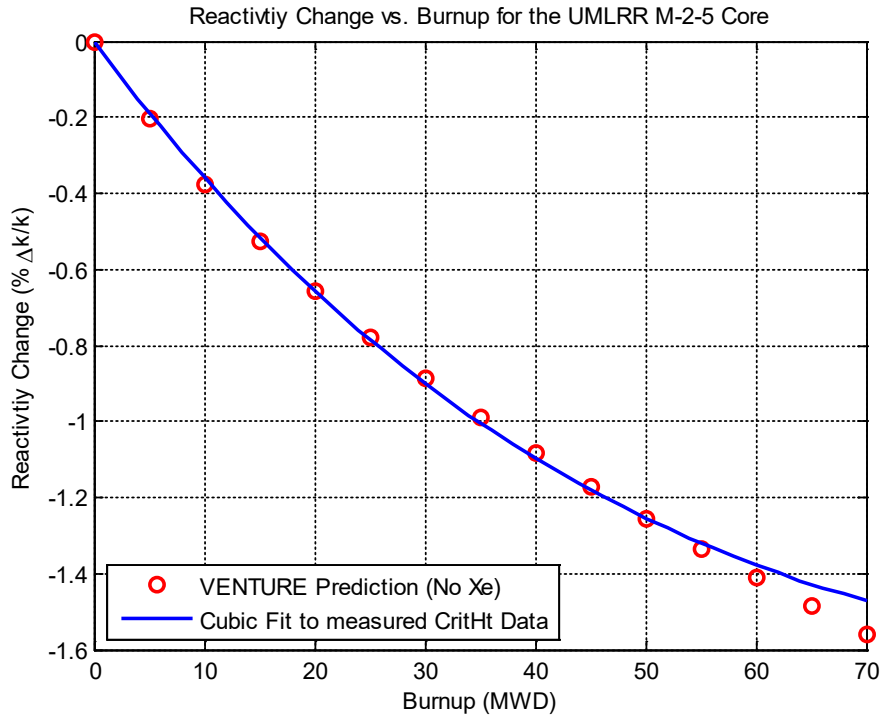

Fig. 17 Reactivity change vs. burnup for the UMLRR M-2-5 core.

Facility Response RAI SAR 4.1 items (c) and (d):

The VENTURE code does not output a summary map of assembly powers or peaking factors. Instead, the code creates interface files that include information about the pointwise flux and power distributions. As a result, the user must do post-processing as necessary for a given analysis situation. At UMass-Lowell, several Matlab-based programs have been written to process both the flux and power density files from VENTURE and to present the information to the user in various ways. Concerning the power maps and peaking factors, the following equations are utilized to obtain the desired information:

power in assembly a: $$P_a = \sum_{ijk \in a} P_{ijk} V_{ijk}$$

where P_{ijk} = node power density and V_{ijk} = node volume

assembly peaking factor: $$f_a = \frac{\text{power in assembly}}{\text{average assembly power}} = \frac{P_a}{P_{tot}/(\#\ \text{assy})}$$

linear heat rate in a for axial level k: $$q'_a\big|_k = \frac{1}{\Delta z_k} \sum_{ij \in a} P_{ijk} V_{ijk}$$ (note the sum is only over i & j)

average linear heat rate in assembly a: $$q'_a\big|_{ave} = \frac{P_a}{H}$$

normalized axial shape function in a: $$\psi_a\big|_k = \frac{q'_a\big|_k}{q'_a\big|_{ave}}$$

Note: $$\langle \psi_a \rangle = \frac{1}{H} \sum_k \psi_a\big|_k \Delta z_k = \frac{1}{H} \frac{H}{P_a} \sum_k \frac{1}{\Delta z_k} \left(\sum_{ij \in a} P_{ijk} V_{ijk} \right) \Delta z_k = 1$$

axial peaking factor in assembly a: $$f_{za} = \max\left\{ \psi_a\big|_k \right\}$$

total intra-assembly peaking factor: $$f_{xyza} = \frac{\max\left\{ P_{ijk \in a} \right\}}{P_a / V_a}$$

intra-assembly radial peaking factor: $$f_{xya} = \frac{f_{xyza}}{f_{za}}$$

axial linear heat rate in hot plate: $$q'_k\big|_{hot} = f_a\, f_{xya}\, \psi_a\big|_k\ q'\big|_{ave}$$

average linear heat rate: $$q'\big|_{ave} = \frac{P_{tot}}{(\#\ \text{plates}) \times H}$$

Note: The hot assembly is defined as the fuel element that generates the most power (i.e. has the largest f_a value). The overall radial peaking factor is given by $f_{xy} = f_a \times f_{xya}$ for the hot assembly. The power generated in the hot plate is f_{xy} in the hot assembly times the average power per fuel plate.

The reference core configuration for the safety analysis was chosen to be the 21-element configuration (designated M-2-5) as shown in the sketch below. This configuration includes 2 partial and 19 full U_3Si_2-Al fuel elements and it has a graphite radiation basket (GRB) in the D5 central location that was designed specifically to minimize the local power peaking in the fuel assemblies next to this element (specifically in locations D4, D6, and E5). A minimum 21-element configuration is needed for routine operation to give sufficient excess reactivity and to make sure that the regulating blade (a.k.a. regulating rod) has sufficient worth to control reactivity changes during normal operation. In addition, we know that the more severe power peaking condition is associated with the blades inserted substantially into the core. Thus, a BOL arrangement with a high excess reactivity which is made nearly critical via blade insertion often gives the desired limiting peaking factors. For the M-2-5 core, the BOL critical height was approximately 14.9 inches withdrawn, and this blade location was used in all the safety studies to be sure to maximize the computed peaking factors.

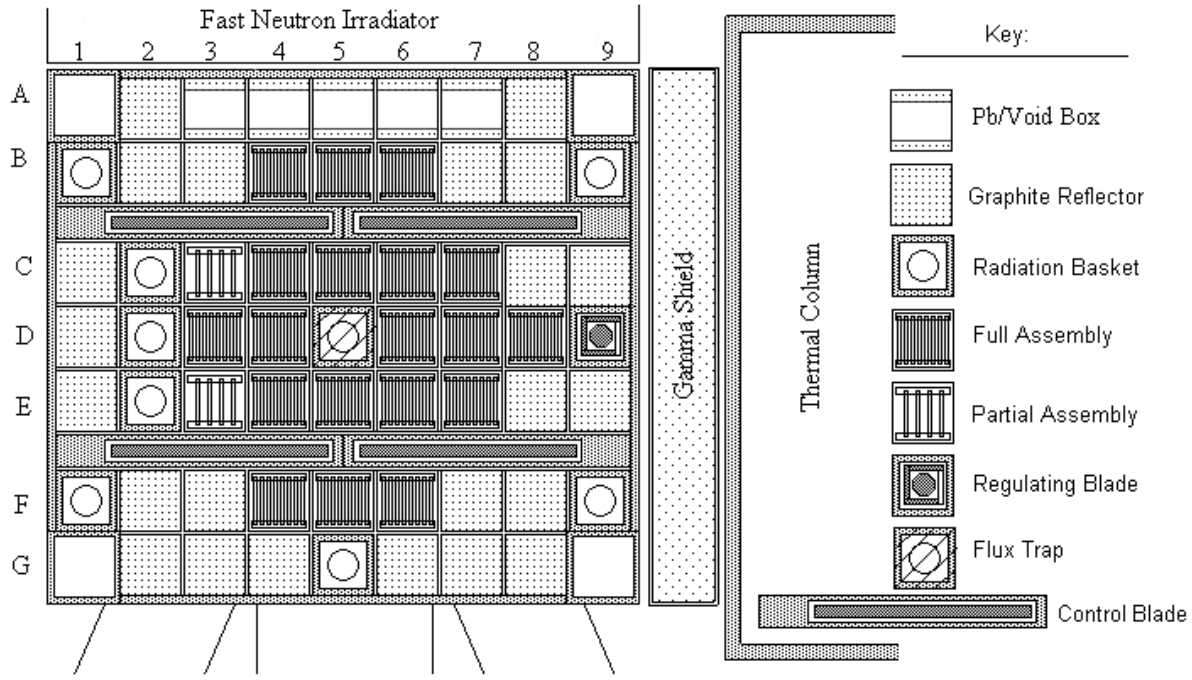

Rough sketch of the M-2-5 core configuration for the UMLRR.

However, the reference core configuration does not represent the worst case configuration. In particular, it is understood that the maximum peaking factors are strongly affected by the design of the experimental element that is placed in the central D5 flux trap location. In this location, the standard water radiation basket (WRB) design gives the largest thermal fluxes and flux gradients, leading to the highest power peaking in the nearby fuel elements. Although a WRB in D5 is not the best option for routine operation, we wish to keep this option available if needed for a specific experiment, so the WRB design was selected for determining the worst case situation.

Within these considerations, the 3-D VENTURE model was used to evaluate a variety of core configurations containing all UMLRR fuel, all WPI fuel, and a mix of both fuel types. Of the

many feasible configurations investigated, the worst case core layout that was identified included a BOL 21-element core with the blades at 14.9″ out, a WRB in D5, eight (8) fresh UMLRR uranium silicide elements immediately surrounding the D5 position (i.e. the inner ring of fuel) and, to emphasize the power peaking in the inner ring, the remaining thirteen (13) elements in the outer ring contained the less reactive WPI uranium aluminide fuel assemblies. Although rather contrived, this is a feasible configuration and it had the largest computed peak power density, with a radial peaking factor of f_{xy} = 1.993 and an axial peaking factor of f_z = 1.383. With these values as a base, it was recommended that these peaking factors both be increased by 5% and rounded up to obtain two significant figures for the quoted values of f_{xy} and f_z. This approach adds some conservatism and gives recommended worst-case peaking factors of about f_{xy} = 2.1 and f_z = 1.5. These values, which combined leads to a total peaking factor of over 3.1, are the peaking factors used in our subsequent NATCON, PLTEMP, and PARET safety analysis calculations.

For comparison purposes, the reference core M-2-5 power maps and the limiting core configuration (LCC) power maps are given below, where these maps only include rows B – F and columns 2 – 8, since there are typically no fuel elements in the outer ring of core grid locations. As apparent, the hot element occurs in location D6 in both cases, but the LCC case (as described above) gives a much larger peaking factor than the reference M-2-5 core, as expected (and as designed). This was the worst case power distribution that was observed out of the large set of feasible core configurations investigated as part of the safety analysis.

Finally, to be specific about the axial power profile, the fuel element in location B5 in the reference M-2-5 core has an axial peaking factor of approximately 1.50 -- thus the axial power distribution in this location was selected for use in the thermal analysis codes. In the code models, 20 discrete axial intervals are used (21 points), so the VENTURE-calculated profile was normalized and then interpolated to the 21 points used within the thermal codes, as shown in the sketch to the right. This axial profile was used for all the subsequent thermal calculations. For an average channel analysis, the values shown were used as displayed along with the average plate power. However, for a hot channel analysis, the values shown were multiplied by the radial peaking factor, f_{xy} = 2.1, to represent the axial profile in the hottest fuel plate in the core.

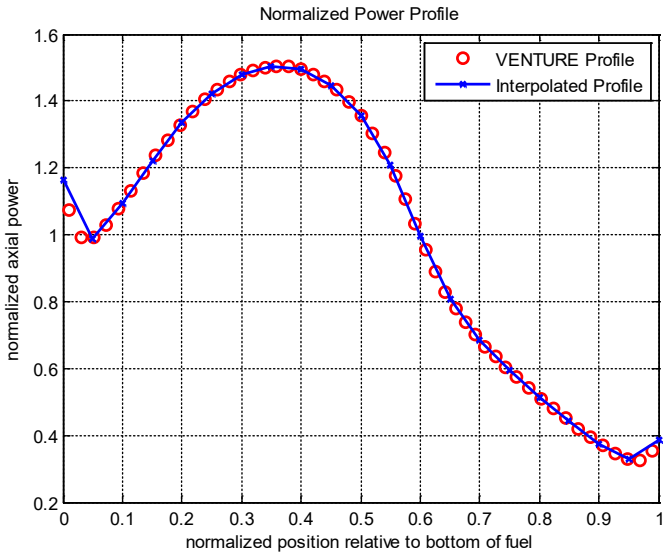

Normalized axial profile used in all safety analyses.

Reference M-2-5 Core Configuration Power Maps (21 elements)

```
Power (kW) by assembly (1 MW total):
 0.000  0.000 28.656 32.076 31.773  0.000  0.000
 0.000 28.410 53.378 62.646 59.407 48.493  0.000
 0.000 46.488 60.687  0.000 68.051 54.034 36.380
 0.000 29.755 56.334 66.145 62.558 50.645  0.000
 0.000  0.000 38.010 43.894 42.179  0.000  0.000

Assembly Peaking Factors by assembly:
 (fa = assembly power/average assembly power)
 0.000  0.000  0.602  0.674  0.667  0.000  0.000
 0.000  0.597  1.121  1.316  1.248  1.018  0.000
 0.000  0.976  1.274  0.000  1.429  1.135  0.764
 0.000  0.625  1.183  1.389  1.314  1.064  0.000
 0.000  0.000  0.798  0.922  0.886  0.000  0.000

AXIAL Peaking Factors by assembly (fza):
 0.000  0.000  1.513  1.504  1.515  0.000  0.000
 0.000  1.455  1.452  1.446  1.449  1.449  0.000
 0.000  1.376  1.373  0.000  1.371  1.370  1.422
 0.000  1.468  1.465  1.459  1.462  1.462  0.000
 0.000  0.000  1.529  1.521  1.527  0.000  0.000

RADIAL Intra-Element Peaking Factors by assembly:
 (fxya = fxyza/fz where fz = fza from above)
 0.000  0.000  1.751  1.696  1.684  0.000  0.000
 0.000  1.179  1.240  1.214  1.197  1.289  0.000
 0.000  1.221  1.280  0.000  1.218  1.213  1.320
 0.000  1.221  1.284  1.183  1.241  1.334  0.000
 0.000  0.000  1.547  1.451  1.487  0.000  0.000

MAX Radial Peaking Factor by assembly (fa * fxya):
 0.000  0.000  1.054  1.142  1.124  0.000  0.000
 0.000  0.703  1.390  1.597  1.494  1.313  0.000
 0.000  1.192  1.632  0.000  1.741  1.376  1.008
 0.000  0.763  1.519  1.643  1.630  1.419  0.000
 0.000  0.000  1.235  1.337  1.317  0.000  0.000
```

Limiting Core Configuration Power Maps (21 elements)

```
Power (kW) by assembly (1 MW total):
 0.000  0.000 27.393 29.467 29.067  0.000  0.000
 0.000 40.300 54.428 65.534 58.315 43.825  0.000
 0.000 45.495 64.980  0.000 69.602 48.213 31.823
 0.000 42.186 57.425 69.196 61.429 45.794  0.000
 0.000  0.000 36.431 40.422 38.673  0.000  0.000

Assembly Peaking Factors by assembly:
 (fa = assembly power/average assembly power)
 0.000  0.000  0.575  0.619  0.610  0.000  0.000
 0.000  0.846  1.143  1.376  1.225  0.920  0.000
 0.000  0.955  1.365  0.000  1.462  1.012  0.668
 0.000  0.886  1.206  1.453  1.290  0.962  0.000
 0.000  0.000  0.765  0.849  0.812  0.000  0.000

AXIAL Peaking Factors by assembly (fza):
 0.000  0.000  1.522  1.513  1.523  0.000  0.000
 0.000  1.458  1.458  1.455  1.456  1.456  0.000
 0.000  1.380  1.385  0.000  1.383  1.375  1.434
 0.000  1.470  1.471  1.467  1.468  1.468  0.000
 0.000  0.000  1.536  1.529  1.535  0.000  0.000

RADIAL Intra-Element Peaking Factors by assembly:
 (fxya = fxyza/fz where fz = fza from above)
 0.000  0.000  1.664  1.622  1.627  0.000  0.000
 0.000  1.224  1.325  1.290  1.290  1.258  0.000
 0.000  1.141  1.403  0.000  1.364  1.205  1.277
 0.000  1.269  1.287  1.251  1.254  1.301  0.000
 0.000  0.000  1.470  1.388  1.436  0.000  0.000

MAX Radial Peaking Factor by assembly (fa * fxya):
 0.000  0.000  0.957  1.004  0.993  0.000  0.000
 0.000  1.036  1.514  1.775  1.579  1.158  0.000
 0.000  1.090  1.914  0.000  1.993  1.220  0.853
 0.000  1.124  1.552  1.818  1.618  1.251  0.000
 0.000  0.000  1.124  1.178  1.166  0.000  0.000
```

Facility Response RAI SAR 4.1 item (e):

The statement in the SAR that the UMLRR U_3Si_2-Al fuel is more limiting than the Worcester Polytechnic Institute (WPI) UAl_x-Al fuel is easily justified. The UMLRR fuel assembly is more reactive (i.e. has a higher k_∞) and it has fewer fuel plates per assembly. This leads to higher powered assemblies when placed into a given core configuration and, for a given assembly power, to a higher plate power since there are only 16 plates per element in the UMLRR assembly (versus 18 fuel plates per WPI element). In particular, Ref. 8 does a detailed comparison with MCNP of the different fuel elements available for use within the UMLRR, and Table 5 below shows the summary results which clearly show that the UMLRR full fuel element is the more reactive of the available assemblies.

The following table (Table 5) is directly from Ref. 8

Table 5 MCNP k_∞ values for the three assembly designs.

Parameter	WPI Fuel Assembly (167 g U235)	UMLRR Full Element (200 g U235)	UMLRR Partial Element (100 g U235)
k_∞	1.5384	1.5670	1.3715
std. dev.	0.00025	0.00026	0.00023
H/U235 ratio	326	292	585

In addition, for the same assembly-average power level (1 MW/21 elements = 47.62 kW) and peaking factors (f_{xy} = 2.1 and f_z = 1.5), PLTEMP computations show that the total core flow rate needed to prevent the onset of nucleate boiling (ONB) in the hot channel (including hot channel factors) is about 536 gpm for the UMLRR assembly design, whereas it only takes a flow rate of about 435 gpm to stay below the ONB point for the WPI fuel design. Furthermore, Tables 4-12 and 4-13 directly from Section 4.6.1 of the SAR (as copied below) also show this same conclusion at a power level of 2.5 MW for forced flow mode, as well as a similar end result using NATCON for the case of natural convection flow.

Thus, in all cases, the UMLRR U_3Si_2-Al fuel element is clearly more limiting than the WPI UAl_x-Al assembly design from both a reactivity perspective and due to the fact that the power per plate is larger.

Table 4-12 ONB flow rate data for P = 2.5 MW for both UMLRR and WPI fuel. (from SAR section 4.6.1)

Case Description	UMLRR Fuel	WPI Fuel
nominal best-estimate calculation	909 gpm	744 gpm
with hot channel factors from Table 11	1561 gpm	1312 gpm

Table 4-13 ONB power levels for free flow for both UMLRR and WPI fuel. (from SAR section 4.6.1)

Case Description	UMLRR Fuel	WPI Fuel
nominal best-estimate calculation	392 kW	466 kW
with hot channel factors from Table 11	248 kW	313 kW

References to support the responses for RAI SAR 4.1:

1. "Report on the HEU to LEU Conversion of the University of Massachusetts Lowell Research Reactor," submitted to the US Nuclear Regulatory Commission in fulfillment of Amendment No. 12 to License No. R-125 (April 2001).
2. J. R. White and L. Bobek, "Startup Test Results and Model Evaluation for the HEU to LEU Conversion of the UMass-Lowell Research," 24th International Meeting on Reduced Enrichment for Research and Test Reactors (RERTR 2002), San Carlos de Bariloche, Argentina (Nov. 2002).
3. J. R. White, A. Jirapongmed, L. Bobek, and T. M. Regan, "Design and Initial Testing of an Ex-Core Fast Neutron Irradiator for the UMass-Lowell Research Reactor," 2002 ANS Radiation Protection and Shielding Topical Conference, Santa Fe, NM (April 2002).
4. J. R. White, L. Bobek, and T. M. Regan, "Initial Testing of the New Ex-Core Fast Neutron Irradiator at the UMass-Lowell Research Reactor," UMass-Lowell internal project documentation (June 2002).
5. J. R. White, R. Gocht, and M. Ducey "Final Report on MCNP Modeling for the UMLRR and Selected Gamma Irradiation Facilities," UMass-Lowell internal project documentation (Sept. 2011). Also see a series of internal Progress Reports that document the on-going development of the MCNP UMLRR model dated Nov. 2010, Jan. 2011, and Aug. 2011.
6. J. R. White, R. Gocht, M. Pike, and J. Marcyoniak, "Validation of the 3-D VENTURE and MCNP UMLRR Core Models used in Support of the WPI Fuel Transfer Project", Research Reactor Fuel Management Conference (RRFM2012), Prague, Czech Republic (March 2012).
7. J. R. White, J. Marcyoniak, and M. Pike, "Overview and Validation of the VENTURE Core Models used in Support of the WPI Fuel Transfer Project," UMass-Lowell internal project documentation (Sept. 2012).
8. J. R. White and J. Marcyoniak, "Comparison of the WPI and UMLRR Fuel Assembly Models," UMass-Lowell internal project documentation (July 2011).

Facility Response RAI SAR-4.2 items (a) and (b):

For the UMLRR safety analysis, the limiting criteria for both steady state operation and for credible off-normal protected transients is the onset of nucleate boiling (ONB) point. Since the coolant saturation temperature for roughly 24 ft of water above the core (i.e. for P = 25 psia or 0.173 MPa) is about 116 C, the ONB point is typically reached at a plate surface temperature of 118 – 125 C depending on the heat flux and flow conditions. Thus, if the maximum clad temperature never exceeds about 125-130 C, there is no possibility of clad or fuel damage in the system. Fuel damage occurs with blister formation, and the blister threshold temperature for both uranium silicide and uranium aluminide fuel is above 500 C, so a maximum clad temperature in the range of 125-130 C guarantees that fuel damage will not occur. Although the ONB condition is a very conservative safety limit, this criteria has been used in all previous safety analyses for the UMLRR and it has not placed undue limits on operation of the reactor for the past 40 years. Thus, this same condition was used for all the safety analyses for the current UMLRR SAR (dated Oct. 2015).

With the specified ONB limit, the subject of flow instability and the onset of flow instability were not addressed at all within the SAR because this condition occurs above the ONB point. Thus, additional information about this subject is not needed for review and evaluation of the UMLRR SAR.

Also, with ONB as the limiting point for operation, the only heat transfer correlations needed in the SAR analyses included the Seider-Tate relationship for the turbulent-flow single-phase heat transfer coefficient and the Bergles-Rohsenow correlation for the onset of nucleate boiling (ONB). These were used consistently in all the PLTEMP and PARET computations reported within the UMLRR SAR. For the natural convection analysis within NATCON, an average of the analytical constant temperature and constant heat flux Nusselt number relationships for laminar flow in rectangular channels was used to obtain the single-phase heat transfer coefficient and the Bergles-Rohsenow correlation was used for prediction of the ONB point.

Facility Response RAI SAR-4.2 item (c):

The NATCON and PARET simulations only modeled the hot plate. Non-uniform heating from plate to plate was not treated in these models. For the steady state ONB analysis in PLTEMP, a full assembly with 18 plates was modeled. For this situation, two different configurations were considered. One model included all heated plates as the "hot" plate with the maximum radial peaking of $f_{xy} = 2.1$ applied to every plate. Since this seemed overly conservative, a second model was constructed where the radial peaking factor varied from the maximum of 2.1 down to 1.5 over a 7-plate span, where the 1.5 value for all the remaining plates represents the average assembly peaking factor for the hot assembly rounded up to two significant figures -- that is, $1.462 \approx 1.5$). However, it turns out that this level of detail was not really needed since the two computations (i.e. constant vs. variable power distribution within an assembly) give quite similar results. For example, for the 1 MW case with no hot channel factors applied, a core flow rate of 314 gpm was required to remain just below ONB for the case with variable plate powers, but with all the plates having an f_{xy} of 2.1, the minimum flow rate needed to stay below ONB only increased to 339 gpm -- which is not a significant increase. Nevertheless, the variable plate power case seemed to be more representative of the real behavior within a UMLRR fuel assembly, so the results from this model were reported within the UMLRR SAR for the PLTEMP steady state ONB analysis. However, as noted above, the NATCON and PARET hot channel analysis results implicitly assume that the neighboring plates produce the same amount of power so that these "hot channel models" effectively represent the case with uniform plate powers within the assembly. Thus, the PLTEMP results use a variable plate power model and the NATCON and PARET results assume a uniform plate power model.

Facility Response RAI SAR-4.2 items (d) and (f):

The PLTEMP code models a steady state system with forced convection flow. The code was used to simulate pump flow through the entire reactor core to determine the amount of flow in the fuel vs. the bypass channels (control regions, experimental basket elements, etc.). In addition, it was also used to do a hot channel analysis to determine the thermal characteristics of the fuel, clad, and coolant as a function of power level and flow rate -- all at steady state forced flow conditions. The hot channel analysis in PLTEMP was used to determine a power-to-flow

map to identify, at a given power level, what flow rate would lead to ONB conditions (this is done by increasing the core ΔP and corresponding flow rate until ONB is no longer exceeded).

Thus, the PLTEMP code was used for two types of analyses that are discussed within the UMLRR SAR, as follows:

1. A full-core model was developed to obtain the flow distribution information needed to determine the fraction of core flow that goes through a single fuel element as a function of the number of fuel elements in the core, and
2. A hot assembly model with 18 individual plates was developed to determine the minimum flow rate needed to prevent ONB as a function of the core power level.

The full-core model used a radial peaking factor of 1.0 to represent that each assembly was at its average power level and the hot assembly model used the maximum f_{xy} of 2.1 for the hot plate with a distribution of plate relative powers varying from 2.1 to 1.5 (as discussed above for RAI #2 item c for SAR Section 4). The full-core model includes three axial regions for the fuel assemblies (top end box, middle fuel region, and bottom grid plate region) and three bypass element types (5 radiation baskets, 4 control blades, and 1 regulating blade). The goal of this model was simply to determine the flow distribution between the fuel elements and the bypass elements as a function of the number of fuel elements in the core. The hot assembly model, on the other hand, models a single assembly with more detailed radial and axial power profiles so that the flow condition that leads to ONB in the hot channel can be determined.

Thus, the full core PLTEMP model contains detailed geometry information for several elements in the UMLRR and the hot assembly model adds further information concerning the radial and axial power profiles in this assembly. Combined, the PLTEMP input files for one case from each of these two models should represent a good resource of general geometry information for the UMLRR (as requested in RAI #2 item f for SAR Section 4). In addition, an Excel spreadsheet was also generated to help prepare the PLTEMP inputs for both models (with emphasis on the full core model since the hot assembly model is just a subset of the larger model). This also contains detailed modeling information that should be useful in preparing confirmatory analyses by the NRC or its contractors. Thus, to provide most of the geometry information requested in RAI #2 item (f) for SAR Section 4, the following files (in electronic form) are included with this report, as follows:

flow_dist.xlsx -- Excel file containing all the raw geometry information and processed input data needed to prepare the PLTEMP input for a full core flow distribution calculation

umlrr_flow21.inp -- actual PLTEMP input file for the 21-element full core flow distribution calculation

uml21_plt_onb1MW_whcf.inp -- actual PLTEMP input file for determining the ONB point for the hot assembly when the reactor is operating at 1 MW with hot channel factors included in the model

Detailed investigation of these files, especially the Excel file, should provide most of the modeling information needed for any confirmatory analyses that may be needed.

Finally, in response to the specific question in RAI #2 item (f.iv) for SAR Section 4, we note that the ΔP across the core is a strong function of the core flow rate and number of elements in the

core. For nominal best estimate conditions of 1 MW with 21 fuel elements, 5 radiation baskets and 1700 gpm core flow (and no hot channel factors), the approximate ΔP is about 0.49 psi as computed by PLTEMP. This includes the pressure drop across the full fuel element, including the top end box, central fuel channels, and the lower end box within grid plate structure.

Facility Response RAI SAR-4.2 item (e):

This RAI requested more comprehensive thermal hydraulic information for steady state operation of the limiting core configuration (LCC) at LSSS conditions. To address this request, we include the computed PLTEMP and NATCON fuel, clad, and coolant axial temperature profiles for the four cases noted below:

Case 1 nominal forced convection: P_o = 1 MW, Q = 1700 gpm, T_{in} = 30 C (no HCFs)

Case 2 worst case forced convection: P_o = 1.25 MW, Q = 1370 gpm, T_{in} = 43 C (with HCFs)

Case 3 nominal free convection: P_o = 100 kW, T_{in} = 30 C (no HCFs)

Case 4 worst case free convection: P_o = 125 kW, T_{in} = 43 C (with HCFs)

Cases 1 and 3 represent best estimate behavior (i.e. no hot channel factors were used) at nominal conditions for forced and natural convection flow, respectively. In contrast, Cases 2 and 4 represent forced and natural convection operation at worst-case conditions (25% higher power, high coolant temperature, and low flow rate for the forced flow case) and these cases include the hot channel factors (HCFs) documented in Section 4.6 of the UMLRR SAR. Note, however, that the LCC peaking factors of f_{xy} = 2.1 and f_z = 1.5 were used in all cases.

As apparent from these four cases (recall that the saturation temperature for water at about 25 psia is about 116 C), steady state operation of the UMLRR is well below the ONB point even when we assume that the LCC is at LSSS worst-case conditions.

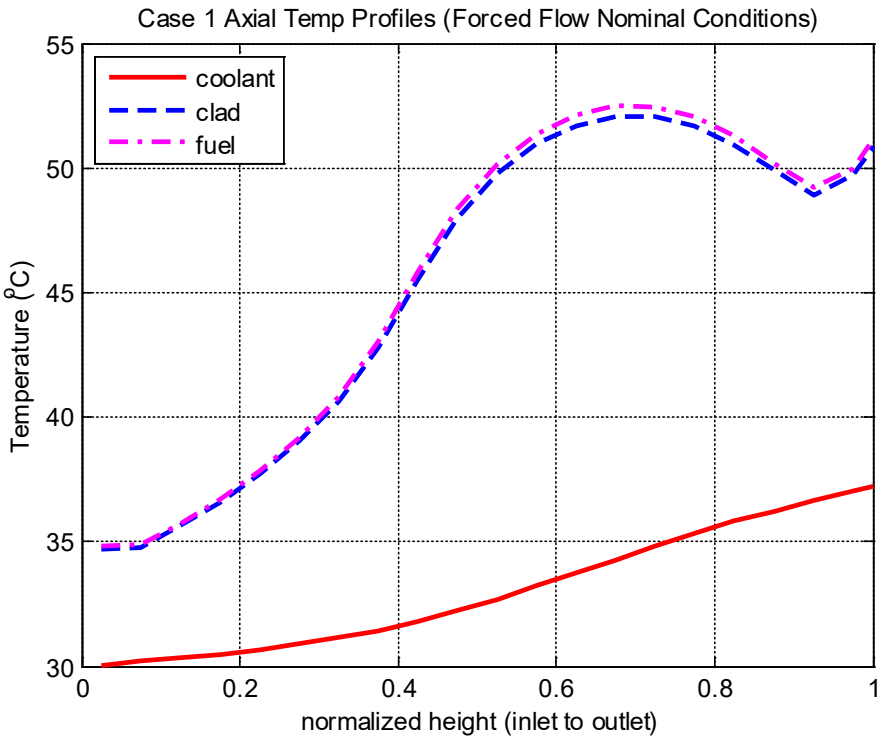

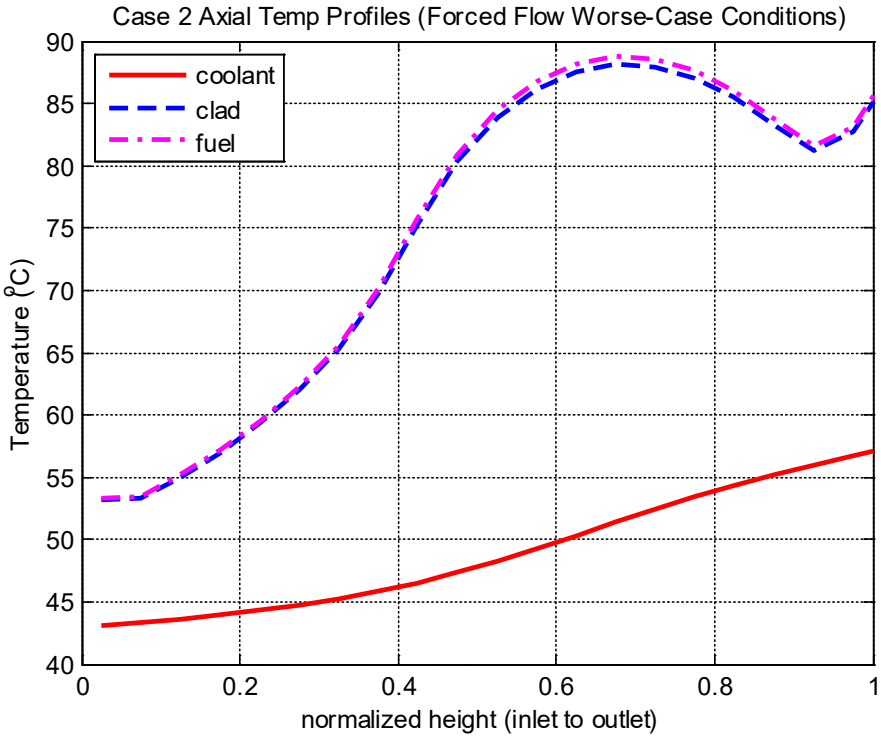

Axial Temperature Profiles for Nominal and LSSS Conditions in Forced Flow Mode

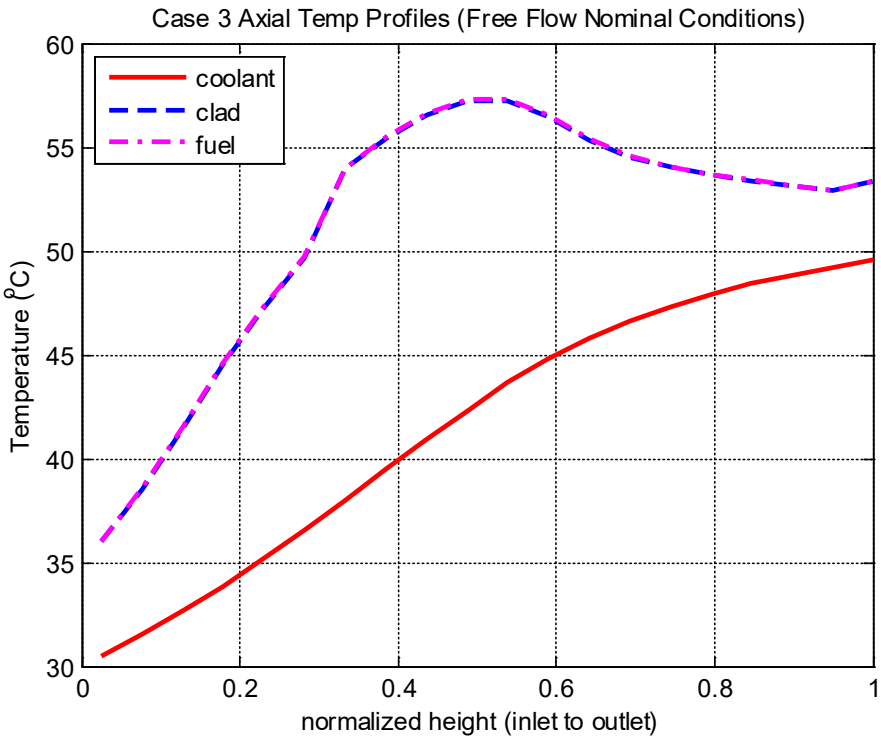

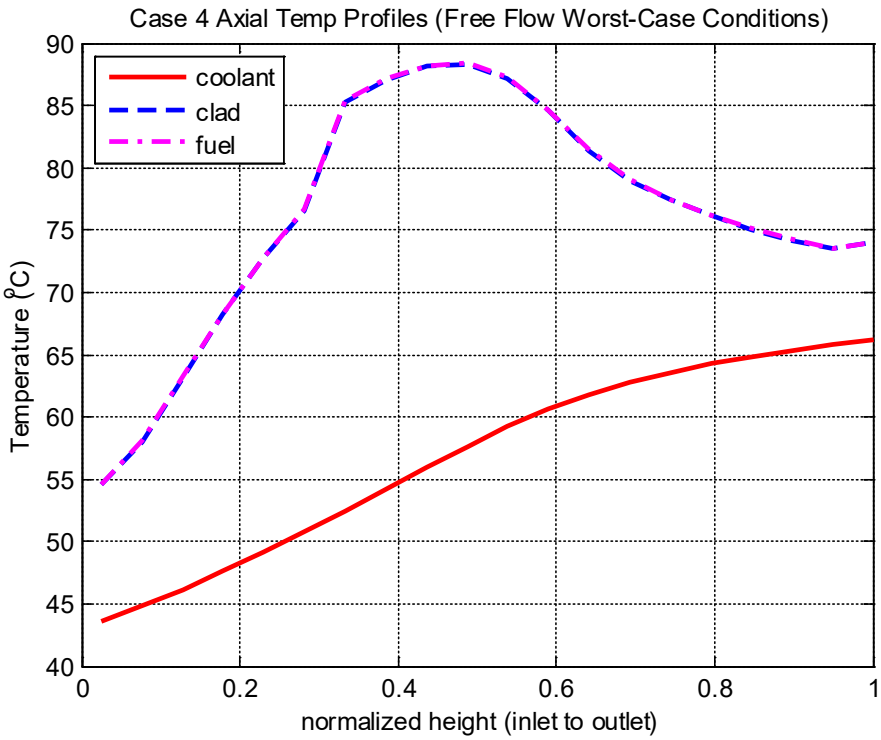

Axial Temperature Profiles for Nominal and LSSS Conditions in Natural Convection Mode

Facility Response RAI SAR-6.1:
The Engineered Safety Feature (ESF) as described in Chapter 6 of the UMLRR SAR is requested to be evaluated as a confinement.

As defined in ANSI/ANS-15.1:

> *Confinement is an enclosure of the overall facility that is designed to limit the release of effluents between the enclosure and its external environment through controlled or defined pathways.*

NUREG 1537-1, 6(1) elaborates further:

> *The confinement is an enclosure of the overall facility (e.g., a reactor room) that is designed to limit the exchange of effluents between the enclosure and its external environment to controlled or defined pathways. A confinement should include the capability to maintain sufficient internal negative pressure to ensure in-leakage (i.e., prevent uncontrolled leakage outside the confined area), but need not be capable of supporting positive internal pressure or significantly shielding the external environment from internal sources of direct radiation.- Air movement in a confinement could be integrated into the HVAC systems, including exhaust stacks or vents to the external environment, filters, blowers, and dampers.*

NUREG 1537-2, 6.2.1 goes on to state:

> *If the HVAC and any air exhaust or liquid release systems associated with the confinement are designed to change configuration or operating mode in response to a potential accident analyzed in Chapter 13 and thereby mitigate its consequences, they should be considered part of the confinement ESF and should be discussed in this section of the SAR.*

The building housing the UML research reactor was designed and built as a containment structure. As such, the UMLRR is one of only three non-power reactors in the United States having a containment building. The others are the University of Missouri-Columbia ($10MW_{th}$) and MIT ($6MW_{th}$). In fact, the UMLRR is the only non-power reactor in the world that is licensed operate at $1MW_{th}$ and is designed with a containment building (ref. IAEA Research Reactor Database).

The UMLRR containment building is described in the SAR Section 3.5.1 and in Chapter 6. The building meets the design features for containment as described in NUREG 1537-1 6(2), including the ability to be sealed to support a defined negative or positive differential pressure. Section 6.2.6 of the SAR provides a summary evaluation of the excursion energy required to achieve a positive differential pressure that is only ¼ of the 2 PSI design basis. It concludes an over-pressurization, even to this relatively low pressure level, is not possible due to an excursion event.

Chapter 13 of the SAR presents multiple scenarios associated with the maximum hypothetical accident (MHA) required by NUREG 1537 to be analyzed for non-power reactor licensing. Scenario-A estimates the dose to personnel inside the building and assumes the automatic shutdown of ventilation (SAR Section 6.2.3) and the emergency exhaust system fails to start (revised SAR Section 6.2.4 below). Scenario-B estimates the dose to the public from the gamma

dose emanating from each of the containment building portals, and assumes the automatic shutdown of ventilation and the emergency exhaust system fails to start. Scenario-C estimates the dose to the public from both the truck door gamma dose and an immersion dose due to a ground level release. The assumptions are an automatic shutdown of ventilation and the emergency exhaust system fails to start. In addition, assumptions are made that there is small positive pressure inside the building and there is leakage at the truck door. Scenario-D assumes a malfunction of the ventilation such that it remains running and does not automatically shut down. Estimated dose to the public is from the truck door gamma dose and an elevated release from the stack. Scenario-E assumes the ESF functions normally and estimates the dose to the public from the truck door gamma dose and an elevated release.

Of these MHA scenarios, Scenario-B represents the most limiting for dose to the public and Scenario-E represents the most likely. For Scenario-B, if an individual where to stand at the entrance to the truck door continuously for a period of 24-hours, the total effective dose equivalent (TEDE) would be 108 mrem, reaching a maximum 123 mrem for a continuous 30-day exposure. At approximately 2.5 meters from the truck door, there is a 4-ft high chain-link fence and a vehicle crash beam that limits public accessibility to the truck door (Figure 6.1.1). At this distance, the maximum TEDE is 32 mrem for a 24-hour continuous exposure and 36 mrem for a continuous 30-day exposure. Doses at the other portals and the containment wall are negligible. Under Scenario-E, the EES operates normally and exhausts the fission products through the stack over an 18 hour period. The maximum TEDE at 2.5 meters from the truck door would be 15 mrem for a continuous exposure over the 18-hour period. All other doses at locations further away are far less or negligible.

Figure 6.1.1

Given the analyses provided in the SAR, the UMLRR ESF is adequate for meeting the requirements specified in NUREG 1537 for confinement.

Based upon the requirements for confinement presented in ANSI/ANS-15.1 and NUREG 1537, a minor modification to the operation of the emergency exhaust system as described in Section 6.2.4 of the SAR is required.

SAR Section 6.2.4 is revised as follows:

6.2.4 Emergency Exhaust System

Under the condition of a GRVS (see previous section), the Emergency Exhaust System (EES) is designed to provide a controlled pathway for the movement of air out of the building and to maintain a negative pressure inside the building. The EES draws air through charcoal filters along with absolute filters into a dedicated duct through a 12-inch blast valve in the building wall. The duct connects to the main exhaust down-stream from all other valves in order to allow passage up the stack. The emergency exhaust fan (designated EF-14 in Figure 6-2) is located above the sample preparation area on the third level of the building and is rated at 320 cubic feet per minute. Electrical power for the EES is supplied by both the normal and the emergency electrical power systems (see Ch. 8). The EES operates independently of the main ventilation system (see sections 6.2.3 and 9.1.1). Automatic or manual operation of the EES is achieved through the Process Control System (see Ch. 7).

Normally, the EES will be in the automatic mode during reactor operation. In this mode, the emergency exhaust fan starts and its associated valve (valve-D) opens under either of two conditions:

(a) the occurrence of a GRVS, or
(b) the differential pressure between the containment building and ambient outside pressure is greater than <u>negative</u> 0.1 +/- 0.05 inch water column.

Operation continues until either:

(c) the GRVS is manually cleared by the operator, or
(d) the differential pressure between the containment building and ambient outside pressure equals or exceeds <u>positive</u> 0.50 +/- 0.05 inch water column.

The emergency exhaust system is designed to maintain negative pressure or relieve small overpressures by exhausting the building air, whether or not accompanied by airborne radioactivity, through a high efficiency particulate filter and then through a charcoal filter before releasing the air to the stack. Emergency exhaust air carried to the stack is diluted by the high volume of air being fed up the stack from the main intake supply fan through the bypass valve F. If condition (c) is met, the emergency exhaust fan stops and valve D closes. The EES remains shut down unless the differential pressure again rises above negative 0.1 +/- 0.05 inch water column.

In the unlikely event of a substantial pressure surge (greater than <u>positive</u> 0.50 +/- 0.05 inch water column), unloading of the excess pressure through the charcoal filter is prohibited since the capacity and effectiveness of the filter is not intended for large volume releases. If

condition (d) is met, the emergency exhaust fan stops and valve D closes. The EES remains shut down until the pressure drops to less than positive 0.50 +/- 0.05 inch water column, at which point the emergency exhaust fan starts and valve D opens. Thus, an overpressure in the building of greater than a half inch water column prohibits release through the stack.

End- SAR Section 6.2.4 (revised)

For the purposes of this revision, the EES requires a simple modification to automatically start when either condition (a) or (b) occurs. This modification will be made, tested, and documented under the 10CFR 50.59 process for the current license.

As a non-power reactor licensed to operate at 1MWth, it is reasonable to impose the less cumbrous license technical specifications associated with a confinement building. Changes to the Technical Specifications for confinement shall be included in an upcoming submittal associated with revised Technical Specifications and will include the following:

1.0: Definitions

The ANSI/ANS-15.1 definition for *Containment* and *Containment Integrity* shall be deleted and the definition for Confinement shall be added.

3.4: Heading 3.4 shall be retitled Confinement.

3.4.1: Heading 3.4.1 shall be retitled Operations Requiring Confinement.

3.4.2: Heading 3.4.2 shall be retitled Equipment to Achieve Confinement.

4.4 Heading 4.4 shall be retitled Confinement.

The specifications for confinement limiting conditions of operation and surveillance shall be consistent with ANSI/ANS-15.1.

Facility Response RAI SAR-11.1:
The primary coolant is continuously filtered by mixed-bed deionizer unit to remove impurities in the water (SAR Section 5.4). The primary coolant is radiologically monitored by direct measurement using fixed area radiation detection equipment and by periodic sampling for radionuclide determination. The fixed area radiation monitoring equipment located in proximity to the primary coolant is described in SAR Section 5.2, paragraph 6. Technical Specification 3.6.1 (1d) requires at least one detector monitoring the primary coolant, at the pool level. Direct measurement using fixed area radiation monitoring instrumentation provides an indication and warning of potential radiological hazards associated with external exposure from the presence of radionuclides in the coolant. Periodic sampling and radiochemical analysis provide a method for detecting the presence of radionuclides in the coolant at sensitivities below the 10CFR Part 20 Appendix-B limits.

In 10CFR 20, any nuclide not listed in App-B (TABLE 3) has a limit of $1x10^{-7}$ μCi/ml (ref. 10CFR 20, App.-B footnote "Table 3 Sewer Disposal"). The detectors used for the radiochemical analysis of liquid samples include liquid scintillation counters and a PIPS detector. For a typical sample size (1 liter evaporated sample) and respective count times, the minimum detectable activities (MDA) currently achievable are $1.78x10^{-9}$ μCi/ml and $2.46x10^{-8}$ μCi/ml respectively for each type of detector. The MDA for either is below the regulatory effluent limits, thus demonstrating the detection capabilities for radionuclides in liquid samples.

Technical Specification 3.3(3) provides an MDA and action limit for radioactivity in the primary coolant.

In addition, the following Technical Specifications shall be included in an upcoming submittal associated with a revision to the Technical Specifications.

> 3.3(4) The secondary coolant shall be analyzed for gross activity. The presence of detectable activity in excess of 10CFR 20 (Appendix B, Table 3, 'Sewer Disposal') limits in the secondary coolant shall require isolation of the secondary cooling system until the cause is corrected.

The Technical Specification 4.3(3) shall be revised as follows:

> The radioactivity in the primary and secondary coolant shall be analyzed quarterly.

The bases for 4.3(3) shall be revised as follows:

> The quarterly radionuclide analyses of coolant samples allows for the determination of any significant build-up of radioactivity from the operation of the reactor, leakage of the Co-60 sources, leakage of fuel, or leakage from the primary cooling system into the secondary cooling system. The instrumentation and methods used for the analyses have a minimum detectable activity that is below the regulatory effluent limits. The quarterly frequency is four times greater than that specified in ANSI/ANS-15.1.

Facility Response RAI SAR-13.1:
An analysis of a reactivity insertion accident during reactor startup was not performed as part of the Oct. 2015 Safety Analysis Report (SAR). This omission has been remedied and the rest of this section is focused on the description and analysis of a series of reactivity insertion events during reactor startup. In particular, it is conceivable though improbable that an off-normal reactivity transient could occur during startup due to the failure of a fixed experiment or possibly due to the rapid ejection of an experimental bayonet from one of the in-core radiation baskets, both of which can lead to a rapid reactivity insertion. In addition, operator error or a control rod drive malfunction during reactor startup could lead to a ramp insertion of reactivity while the reactor is initially at a low-power state. Both rapid (near step) and ramp reactivity insertions were analyzed and discussed as part of the Oct. 2015 UMLRR Safety Analysis Report (SAR), but none of the situations addressed started at a low power level -- all the transients were initiated at rated or LSSS power levels.

To address an inadvertent reactivity insertion during startup, a series of PARET simulations were made with an initial power level of P_o = 0.01 W, including both step and ramp insertions under both forced and free flow conditions. In all cases the inlet temperature was at the LSSS value of 43.3 ^oC and, for the forced flow cases, the core flow rate was also at the LSSS value of 1370 gpm (this gives a mass flux of 799.1 kg/s-m^2 down through the core). For the natural convection cases, the initial mass flux was set at 0.001 kg/s-m^2 up through the core since PARET will not execute properly with an initial flow rate set to exactly zero. In all cases, it was assumed that the transient was terminated by the over-power trip signal (1.25 MW for forced flow and 0.125 MW for the natural convection cases) with a 210 msec instrument delay time between when the trip level is exceeded and the blades begin to drop. Though not required by NUREG 1537, this scenario assumes the short period trip is inoperable and not included within any of the simulations.

The UMLRR Technical Specifications set the maximum worth of a single experiment at 5 mk and the maximum ramp reactivity insertion rate at 0.5 mk/s. These specifications are supported by the Oct. 2015 UMLRR SAR which showed that the onset of nucleate boiling (ONB) would not occur at any time during the transient for a 6 mk step insertion or for a 0.7 mk/s ramp insertion rate for both forced and natural convection modes under different initial states (including LSSS conditions). However, as noted above, a low-power startup scenario was not simulated previously. To be consistent with the previous analyses, a 6 mk step insertion and a 0.7 mk/s ramp insertion rate have also been used here for the simulated accidents during reactor startup (with P_o = 0.01 W).

The series of plots shown below summarize the results of the simulated startup accidents and compare these to the corresponding simulations starting at the LSSS power level (1.25 MW for forced flow and 0.125 MW for the natural convection cases). The key difference, of course, is that the over-power trip is reached right away when the initial power is at the LSSS level but, when the initial power is essentially zero, it can take several seconds for the over-power trip to engage, leading to very large power gradients during the simulation. Thus, the PARET runs with the two different starting power levels, although quite similar in all other respects, can show quite different overall transient behavior.

In particular, for the $\Delta\rho$ = 6 mk step insertion cases, when P_o = 0.01 W, the power levels and temperatures spike about 15-20 seconds after the transient is initiated. In contrast, when P_o is the LSSS power level, the transient is essentially over in under 1 second, since the over-power trip is initiated immediately and after about 0.21 seconds due to the instrument delay, the control blades start to drop, terminating the transient. However, as apparent in the comparison plots, the cases with P_o at the LSSS level are more limiting since the peak transient power level and the peak temperatures for both the forced and natural convection simulations are much larger than for the corresponding simulations involving a reactor startup scenario (with P_o = 0.01 W). The most important observation, however, is that none of the 6 mk step insertion simulations reached the ONB limit for the UMLRR. It is clear an experiment malfunction that rapidly inserts a maximum of 5 mk of reactivity will not exceed the ONB limit, independent of the initial power level of the system.

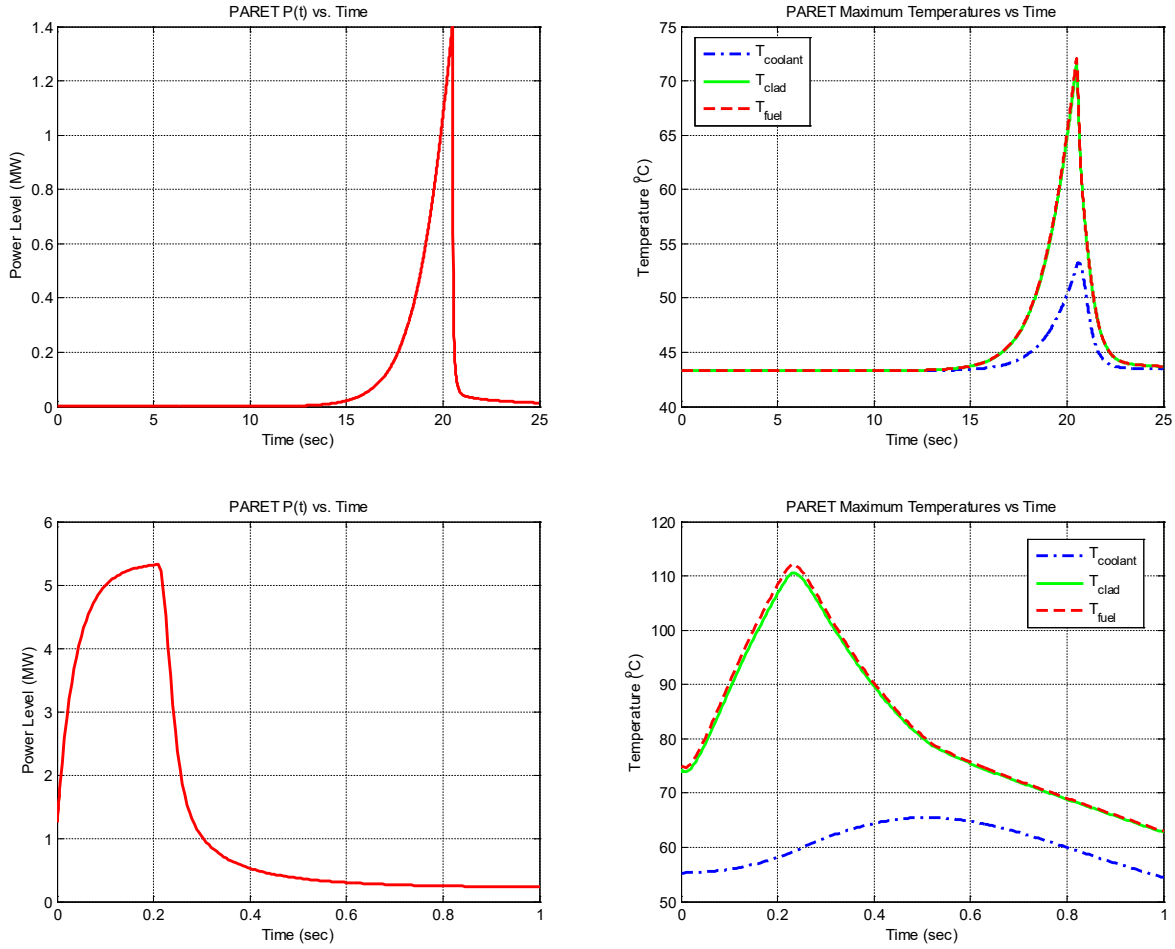

Comparison of transient responses (forced flow mode) for 6 mk step insertion for P_o = 0.01 W (top plots) and P_o = 1.25 MW (bottom plots).

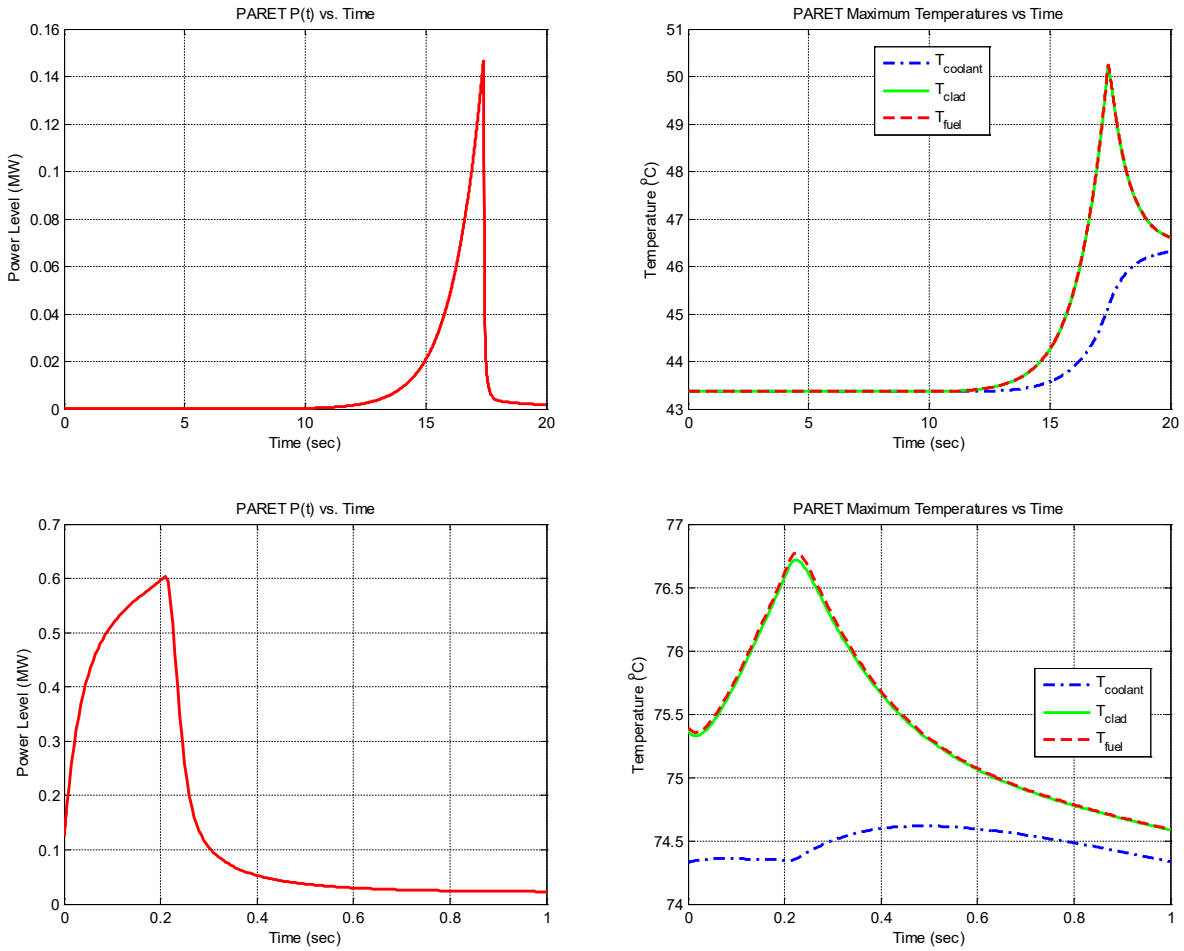

Comparison of transient responses (natural convection mode) for 6 mk step insertion for P_o = 0.01 W (top plots) and P_o = 0.125 MW (bottom plots).

For the ramp insertion cases, the initial conditions are similar, but the results are quite different. For the startup scenarios with P_o = 0.01 W, the powers and temperatures have very sharp spikes about 12 seconds into the transient and, as above, the transient has essentially terminated within 1 second for the cases where P_o is at the LSSS level. However, the key difference here is that the ramp reactivity insertion continues for a relatively long time (about12 seconds) for the reactor startup simulations, and this can lead to a large total reactivity insertion level before the transient is terminated by the over-power trip signal. In fact, a 0.7 mk/s insertion rate over 12 seconds gives $\Delta\rho = 0.0084\ \Delta k/k$, which is over 1$ of positive reactivity for the UMLRR. This creates the very fast power and temperature spikes that are observed for the reactor startup cases. As seen in the comparison plots, the rapid spikes for the startup simulations make these cases more limiting than the corresponding scenarios when P_o is at the LSSS power level.

However, as before, the most important observation is that none of the 0.7 mk/s ramp insertion simulations reached the ONB limit for the UMLRR. The forced convection case was closest with a peak clad temperature of just under 120 ^oC. Nevertheless, these simulations indicate that an accident during startup that leads to a ramp reactivity insertion rate of 0.5 mk/s (the TS limit) will not exceed the ONB limit set for the UMLRR safety analyses.

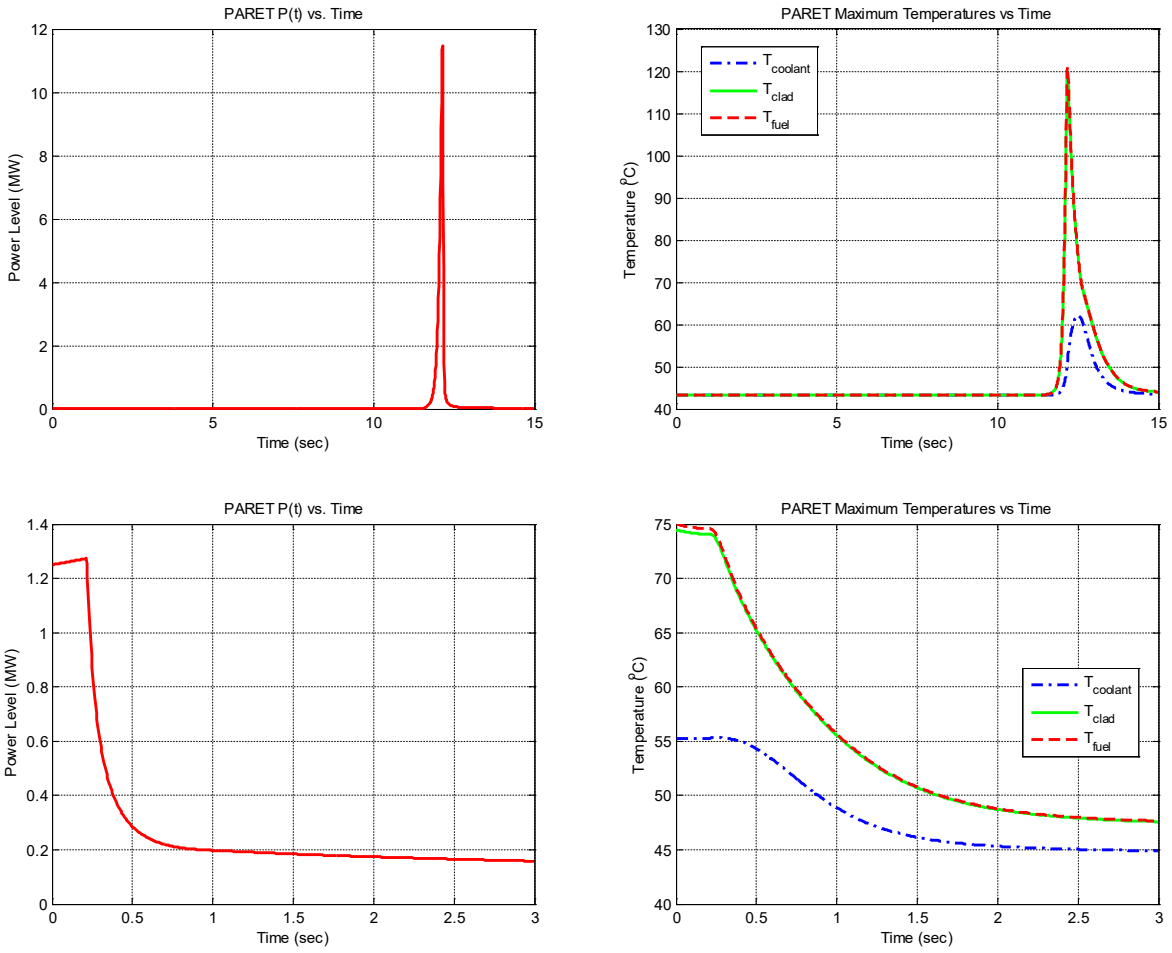

Comparison of transient responses (forced flow mode) for 0.7 mk/s ramp insertion for P_o = 0.01 W (top plots) and P_o = 1.25 MW (bottom plots).

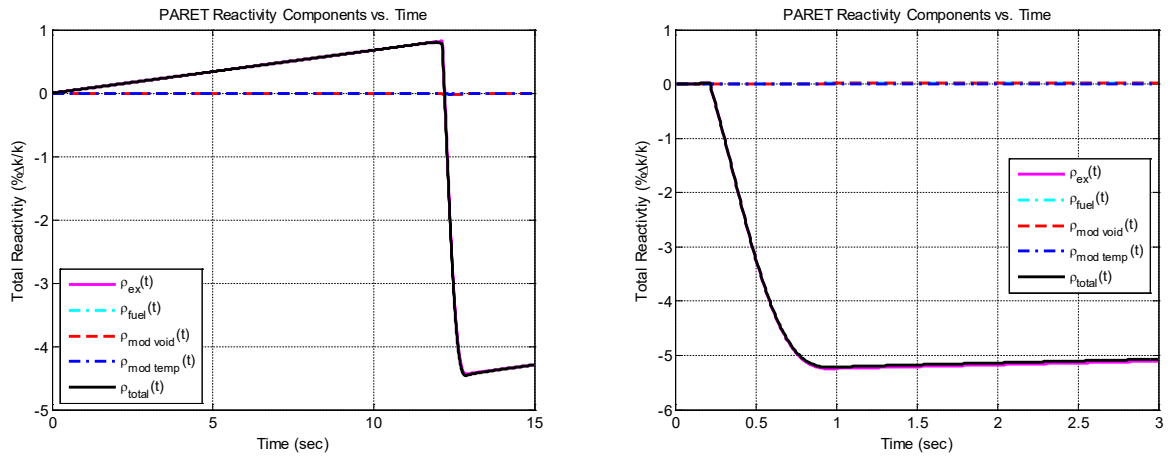

Comparison of reactivity profiles (forced flow mode) for 0.7 mk/s ramp insertion for P_o = 0.01 W (left plot) and P_o = 1.25 MW (right plot).

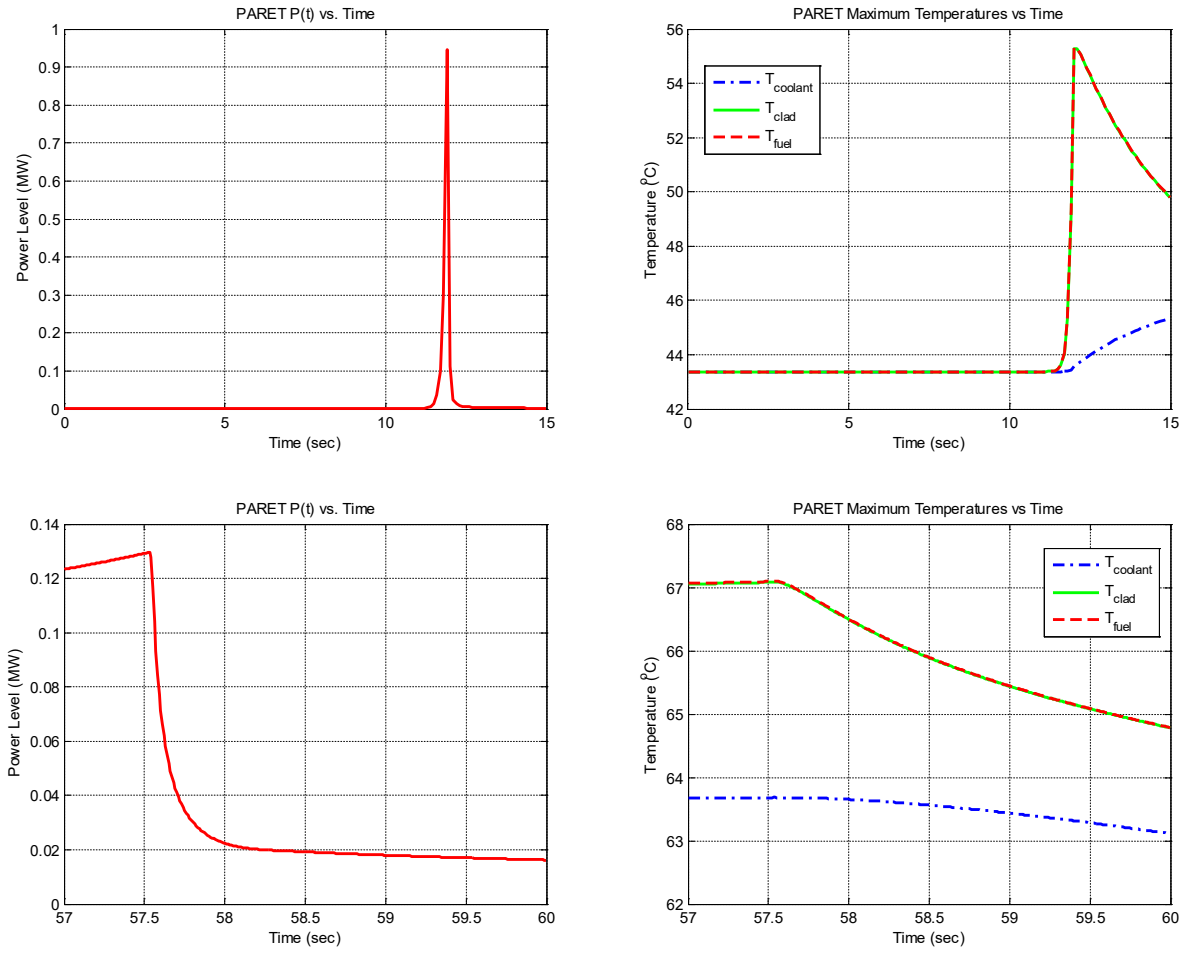

Comparison of transient responses (natural convection mode) for 0.7 mk/s ramp insertion for P_o = 0.01 W (top plots) and P_o = 0.125 MW (bottom plots).

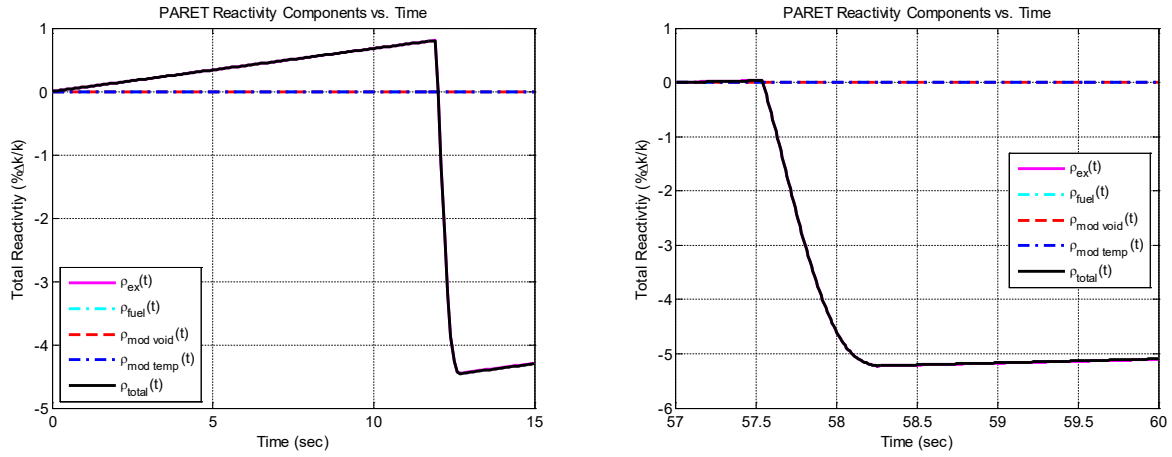

Comparison of reactivity profiles (natural convection mode) for 0.7 mk/s ramp insertion for P_o = 0.01 W (left plot) and P_o = 0.125 MW (right plot).

Facility Response RAI SAR 13.2 items (a), (b), and (d):

A Loss of Coolant Accident (LOCA) at the UMLRR is highly unlikely event due to the design of the facility. The pool is specifically designed to preclude the probability of accidental drainage. It is constructed of reinforced concrete with approximately six-foot thick walls and a heavy aluminum liner to resist the most severe earthquake that might reasonably be expected in the area (SAR Section 3.4).

There is no penetration of the reactor pool below the top of the core that is open to pool water. A guillotine pipe break in the ten-inch diameter primary coolant pipe between the reactor and heat exchanger could not empty the pool. An automatic anti-siphon line is provided in the discharge line of the primary coolant loop. This line is equipped with a break valve located above the reactor pool water level. The break valve will normally be closed by pressure during forced circulation. Loss of pressure will cause the break valve to open. A second anti-siphon open standpipe line is connected to the return primary coolant line. Both anti-siphon risers which connect to the primary system are 3 inch aluminum pipes embedded in the concrete, which are connected to the 10 inch (in concrete) primary lines. The anti-siphon lines extend out of the concrete just above the surface of the reactor pool water. In the event of a primary piping failure, the pool will start to siphon. After the pool level has dropped to the level of the primary pipes (approximately 11-ft above core centerline), air admitted to the anti-siphon risers will prevent a continuing siphon effect.

There are several experimental facilities built into the concrete shielding surrounding the pool liner on the experimental (reactor core) level (SAR Chapter 10). These experimental facilities are provided with multiple barriers against the possibility of pool water leakage. There are also two 6-inch and one 8-inch beam ports (SAR Section 10.2.1) that penetrate the pool liner at core centerline in the stall end of the pool (SAR Section 4.3). Each beam-port precludes accidental drainage by a sealed bolted cap at the pool end, by a heavy lead shutter located within the pool shield wall, and by a bolted shield plug at the outer shield wall. Due to radiological considerations, even after an extended shutdown period, the lead shutter is not raised and the shield plug removed when the reactor is positioned adjacent to experimental facilities in the stall end of the pool.

It is highly unlikely that the beam-ports could be severely damaged by a falling object while the reactor core is in the stall pool due to the restricted space and protection afforded by the reactor bridge (SAR Section 4.2.5). The reactor bridge spans the entire width of the reactor pool and provides support of the reactor core and the core suspension frame, as well as serving as an access platform (Figure 13.2.1). The bridge consists of two separate sections of structural frame work set horizontally one above the other and supported on each side of the pool by a two-wheel, rail-mounted truck assembly. The truck assembly allows the reactor bridge to be positioned at any desired location within the reactor pool. When positioned in the stall pool, the bridge provides for direct vertical protection of the beam-ports (Figure 13.2.1).

An additional and important safety feature is the pool divider gate (Figure 13.2.1) that allows separation of the stall pool from the bulk irradiation pool. The pool divider gate is constructed of reinforced aluminum and is approximately 5 ½ feet wide by 27 feet high. A rubber gasket located around the edges of the gate provides a watertight seal. The gate permits independent drainage of either pool section for maintenance purposes. Similarly, a severe leak in one side of the pool can be prevented from uncovering the core by moving the reactor to the unaffected side

and closing the gate between the two pools -- an operation that can be done in a matter of a few minutes.

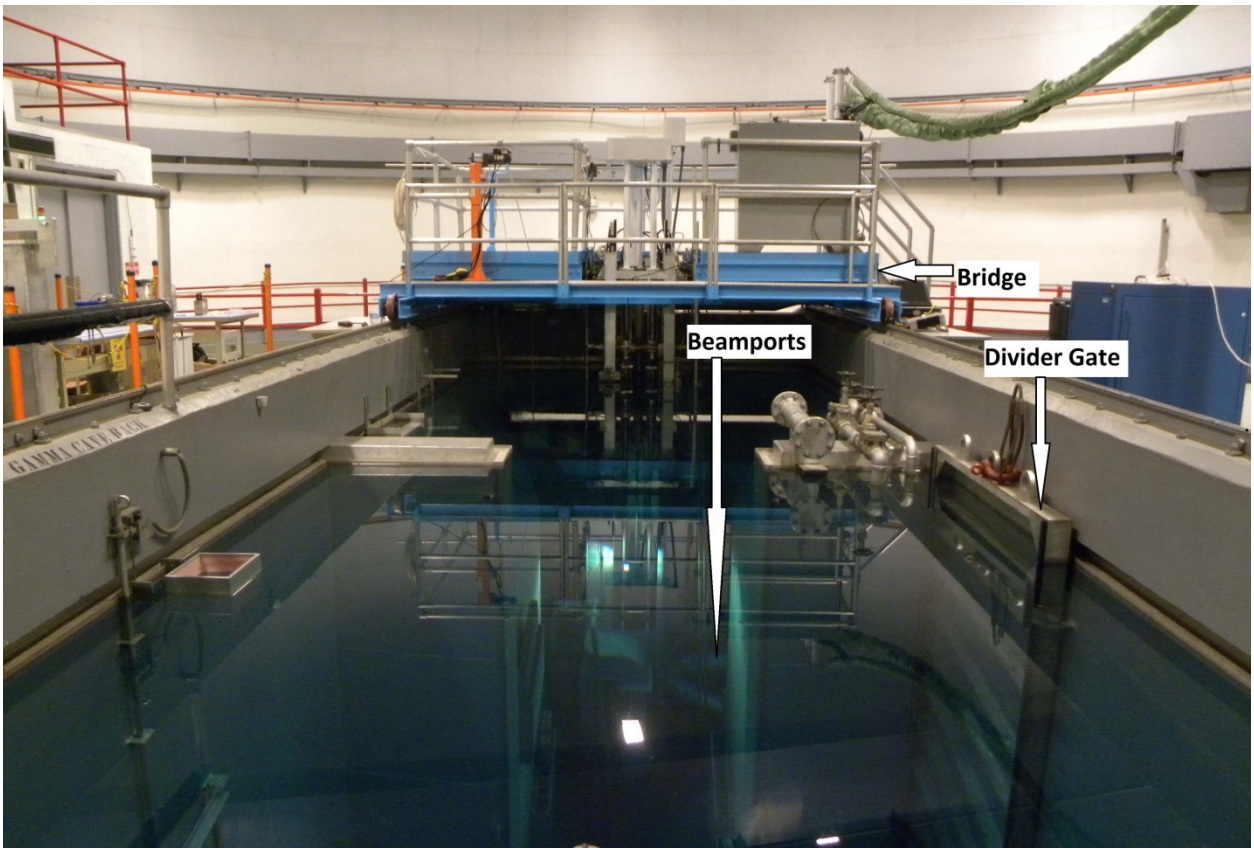

Figure 13.2.1

As indicated above, the inherent integrity of the design features makes a loss of pool water to the point of uncovering some of the core a highly unlikely event. Nevertheless, the following analysis is provided to determine the potential consequences of a LOCA.

To determine the LOCA consequences for the UMLRR, the Rhode Island Nuclear Science Center (RINSC) RINSC LOCA Analysis and the addendum performed by Dr. Earl Feldman of Argonne National Laboratory is referenced. The RINSC analysis is of particular relevance as the RINSC and UMLRR facilities have similar physical characteristics. Both facilities were designed and built by General Electric as open pool reactors utilizing MTR flat-plate fuel. The reactor pool, reactor core support structure, and beam-ports for both facilities have identical characteristics. The commonalities of the two facilities allow for the analyzed thermodynamic conditions for the RINSC reactor to be applied directly to the UMLRR.

There are, however, structural and core differences between the two facilities that affect the possibility and effects of a LOCA at the UMLRR. One is the lack of a through-port assembly. The through-port at the UMLRR was never installed due to concerns it ran underneath the reactor core. The other was the removal of three of the six original beam-port tubes surrounding the UMLRR core to install a fast neutron irradiator system. The affected beam-port tubes were

removed from the pool and replaced with ¾" aluminum blank face plates at the pool wall. In terms of physical core differences, the most significant is that RINSC has a 14 element, beryllium reflected core, while UMLRR is a 21 element graphite/water reflected core. The larger UMLRR core has a lower average and peak power production, making the higher power RINSC analysis more limiting.

A summary of the RINSC analysis states *"the analysis performed by Dr. Feldman (for RINSC) shows that as long as part of the fuel meat remains submerged in water at a level that is no lower than the elevation of the bottom of the eight inch beam ports, and the power fraction is no greater than 0.827%, then there is sufficient cooling capacity to prevent the fuel cladding temperature from reaching the blister point. Conservatively, the drain time has been taken to be the amount of time that it takes for the pool level to drop from the scram set point to the top of the grid box, which is well above the top of the fuel meat.*[1]"

Power Fraction Effect on Fuel Plate Temperature During a LOCA

For the RINSC reactor operation at 2-MW, the highest fuel plate power is 9.653kW[2]. Each of the 14 RINSC fuel elements has 22 fuel plates. The RINSC criteria for damage to fuel, requires that fuel temperature does not exceed 530^{o} C. Based on the analysis by Feldman, the amount of time (after infinite reactor operation) needed for the decay heat production to drop below that necessary to generate temperatures capable of blister for partially submerged fuel is 16,232 seconds (4.5 hours). The partial submerged environment is predicated on water draining to the bottom of the 8" beam port as described in the Feldman reports.

UMLRR has identical physical constraints (pool size, beam-port elevations and fuel element pitch). The thermodynamic initial conditions presented in the RINSC reports are applicable to UMLRR under similar accident conditions. The only geometric differences come from the plate spacing on the RINSC fuel. The RINSC fuel plates are slightly closer than the UMLRR fuel, with UMLRR fuel having 18 plates (2 of which are dummy aluminum plates) compared to the RINSC fuel which has 22 fueled plates. The 2-MW RINSC core contains 14 fuel elements with 308 fuel plates, while the larger UMLRR reference core contains 21 fuel elements with a total of 336 fuel plates (see SAR Chapter 4 and response to RAI SAR-4.1 item c & d).

Based on the larger cell size and lower peak and average power production in the UMLRR core compared to the RINSC core, it is reasonable to conclude the natural convection flow characteristics in the UMLRR core under LOCA conditions would be the same or more conservative than the RINSC core. The channel width of the UMLRR plate fuel is 0.2963 cm vs 0.2620 cm for the RINSC plate fuel, with the fuel meat width of the UMLRR fuel being 0.06085 cm vs 0.06083 cm for RISNC fuel.

The 1 MW UMLRR average plate power for a nominal reactor power of 1MW (equally spread over the 336 fuel plates) is 2.98kW, while the peak plate power is 6.25kW. The UMLRR peak power includes all uncertainties for both the axial and radial peaking factors[3]. Thus, the peak plate power for the UMLRR fuel is less than 0.65 that of the maximum RINSC plate power.

[1] Dr. Earl Feldman, Argonne National Laboratory LOCA Analysis Addendum Rev 2. RINSC pg 13

[2] Dr. Earl Feldman, Argonne National Laboratory prepared a Loss of Coolant Accident Analysis for the Rhode Island Nuclear Science Center in 2004 entitled, "Section 13.2.3 Loss of Coolant Accident (LOCA) of Safety Analysis Report of the Rhode Island Nuclear Science Center Reactor, Submitted May 3, 2004" Table 13.2.3-4

[3] John R. White "Safety Analyses for the UMass-Lowell Research Reactor (UMLRR) 17 Aug 2015, p24 Table 11

Feldman determined that a plate power fraction (as a % of full-power) of 0.827% or less is needed to ensure sufficient cooling of the RINSC core.

Given the peak plate power for the UMLRR fuel is less than 0.65 that of the maximum RINSC plate power, the power factor (as a % of full-power) required to prevent blister damage for UMLRR will be at 1.28% or less. Based on Decay Heat (Fraction of Steady State Power) as Function of Reactor Operation Scenario, ANSI/ANS-5.1-2005 Decay Heat Standard (Table 1, attached), this equates to 3947 seconds, or approximately 66 minutes, after infinite operations for 40 years. It is worthwhile to note that for a more realistic yet still conservative 40 hour/week operation for 40 years, the time necessary for the fuel temperature to be below the blister temperature decreases to 26.6 minutes after shutdown.

Using Feldman's RINSC LOCA Addendum, after infinite operations, it takes 16,232 seconds for the decay power to drop below the point at which the fuel cladding may be damaged at RINSC[4]. The maximum area of a beam port that can be open to confinement, while still providing 16,232 seconds of drain time between the level at which the pool level scram trips, and the top of the grid box was calculated:

$$t_{final} = \frac{2A_1}{C_d A}\left[\sqrt{\frac{h_{initial}}{2g}}\right]\left[1 - \frac{\sqrt{(h_{final})}}{\sqrt{(h_{initial})}}\right]$$

$$A = \frac{2A_1}{C_d t_{final}}\left[\sqrt{\frac{h_{initial}}{2g}}\right]\left[1 - \frac{\sqrt{(h_{final})}}{\sqrt{(h_{initial})}}\right]$$

$$A = \left[\frac{(2)(150\,ft^2)}{(0.61)(16232\,\mathrm{sec})}\right]\sqrt{\left[\frac{(28.06\,ft)}{(2)(32.2\,ft/s^2)}\right]}\left[1 - \sqrt{\frac{(4.84\,ft)}{(28.06\,ft)}}\right]$$

$A_{RINSC} = 1.169 \text{ X } 10^{-2}$ ft^2 = 1.68 in^2

However, the RINSC calculation and basis of the 150 ft^2 pool surface area used in the Feldman analysis is a substantial underestimation of the actual pool surface area. The 150 ft^2 represents only the area of one side of the entire reactor pool surface area. When combined, the overall surface area of the bulk, stall, and gate pool regions exceeds 400 ft^2. As the RINSC Technical Specifications also do not allow for operations with their pool gate (dam) in place (RINSC TS 3.1.2.2), the 150 ft^2 surface is not a reasonable representation of the actual surface area. Given that the sloping sides of the stall pool walls reduces the effective area as the pool drains, a conservative, average surface area of 372 ft^2 is used for the UMLRR analysis[5].

Based on the larger surface area, the refined maximum leakage area for the RINSC facility would increase to:

$A_{RINSC - refined} = 2.900 \text{ X } 10^{-2}$ ft^2 = 4.175 in^2

Substitution of the calculated drain time for UMLRR at 3947 seconds (infinite operation for 40 years), yields a drainage area of:

[4] Dr. Earl Feldman, Argonne National Laboratory LOCA Analysis Addendum Rev 2. RINSC pg 11

[5] UMLRR FSAR September 1973 Chapter 9 pg 20

$A_{UMLRR} = 4.812 \text{ X } 10^{-2} \text{ ft}^2 = 17.17 \text{ in}^2$

This result indicates that even with infinite operations and no mitigation actions taken, UMLRR fuel can remain cooled below the blister point of the fuel with a drainage diameter up to 4.68 in. For the more applicable heat source term of 40 hours per week and 40 years of operation, the diameter of the allowable sheared pipe increases to 7.35 inches.

There are no other pipes (conduit, fill, or drainage) associated with the beam-ports that exceed 4-inches in diameter. A substantial break of a beam-port inside the pool exceeding an equivalent 4.68 diameter, following an equivalent infinite operation, with the reactor in the stall end, the beam-port shutter up, the beam-port plug removed, and no mitigation actions -- all combine to create a non-credible event. Specifically, all other mitigating factors aside, having both the lead shutter raised and the shield plug removed is not practical due to radiological concerns when the reactor is positioned adjacent to the beam-ports.

Facility Response RAI SAR 13.2 items (c) and (e):

The UMLRR facility has a pool level sensor that initiates an automatic pool fill system that operates at a flow rate of up to 5 gpm. This system provides makeup water thought the cleanup demineralizer. The make-up flow is activated by means of an ultrasonic sensor located on the reactor lower bridge. This same sensor and a redundant mechanical float sensor also provide a scram signal to the reactor protection system should the level drop by approximately six inches (Technical Specification 2.2.1(4) LSSS equates to 9-in). A nine inch drop in pool height corresponds to a loss of approximately 2250 gallons of the total 76,000 gallon pool capacity. The pool level sensor is required by T.S. 3.2.3 and its periodic surveillance is required by T.S. 4.2.2. Though not described in the SAR, an additional mitigation mechanism available within containment includes a two inch diameter fire hose that can serve as an emergency pool filling method, rated to supply up to 300 gpm.

Table 1. Decay Heat (Fraction of Steady State Power) as Function of Reactor Operation Scenario, ANSI/ANS-5.1-2005 Decay Heat Standard.

Shutdown time (sec)	*Cyclic Operations*							Infinite Operation (10^{13} seconds)
	40 hrs/wk for ~40 years	72 hrs/wk for ~40 years	120 hrs/wk for ~40 years	168 hrs/wk for ~20 years	168 hrs/wk for ~40 years	168 hrs/wk for 100 years	168 hrs/wk for 1000 years	
0	6.358%	6.473%	6.595%	6.586%	6.698%			
1	5.823%	5.937%	6.060%	6.051%	6.163%	6.181%	6.186%	6.190%
1.5	5.638%	5.752%	5.875%	5.866%	5.978%	5.996%	6.001%	6.005%
2	5.485%	5.600%	5.723%	5.713%	5.825%	5.843%	5.848%	5.850%
4	5.053%	5.167%	5.290%	5.281%	5.393%	5.411%	5.416%	5.420%
6	4.765%	4.880%	5.002%	4.993%	5.105%	5.123%	5.128%	5.130%
8	4.551%	4.665%	4.788%	4.778%	4.891%	4.909%	4.914%	4.917%
10	4.382%	4.497%	4.620%	4.610%	4.722%	4.740%	4.745%	4.749%
15	4.077%	4.192%	4.314%	4.305%	4.417%	4.435%	4.440%	4.443%
20	3.864%	3.979%	4.101%	4.092%	4.204%	4.222%	4.227%	4.230%
40	3.365%	3.480%	3.603%	3.593%	3.705%	3.723%	3.729%	3.732%
60	3.080%	3.195%	3.317%	3.308%	3.420%	3.438%	3.443%	3.446%
80	2.883%	2.997%	3.120%	3.110%	3.222%	3.240%	3.246%	3.249%
100	2.735%	2.850%	2.972%	2.963%	3.075%	3.093%	3.098%	3.101%
150	2.484%	2.599%	2.721%	2.712%	2.824%	2.842%	2.847%	2.850%
200	2.321%	2.435%	2.558%	2.548%	2.660%	2.678%	2.684%	2.687%
400	1.970%	2.084%	2.207%	2.197%	2.310%	2.328%	2.333%	2.336%
600	1.778%	1.892%	2.015%	2.005%	2.117%	2.135%	2.141%	2.144%
800	1.641%	1.755%	1.878%	1.868%	1.980%	1.998%	2.004%	2.007%
1000	1.535%	1.649%	1.771%	1.761%	1.874%	1.892%	1.897%	1.900%
1500	1.341%	1.455%	1.577%	1.567%	1.680%	1.698%	1.703%	1.706%
2000	1.206%	1.319%	1.442%	1.432%	1.544%	1.562%	1.568%	1.570%
4000	0.906%	1.019%	1.141%	1.131%	1.243%	1.261%	1.267%	1.269%
6000	0.757%	0.869%	0.991%	0.981%	1.093%	1.111%	1.117%	1.119%
8000	0.664%	0.775%	0.896%	0.886%	0.998%	1.016%	1.022%	1.024%
10000	0.597%	0.707%	0.828%	0.818%	0.930%	0.948%	0.953%	0.956%
15000	0.488%	0.596%	0.717%	0.707%	0.818%	0.836%	0.842%	0.844%
20000	0.421%	0.528%	0.647%	0.637%	0.748%	0.766%	0.772%	0.775%
40000	0.289%	0.389%	0.505%	0.495%	0.605%	0.623%	0.628%	0.631%
60000	0.227%	0.322%	0.436%	0.426%	0.534%	0.552%	0.558%	0.561%
80000	0.191%	0.282%	0.393%	0.384%	0.490%	0.508%	0.514%	0.517%
100000	0.168%	0.255%	0.364%	0.355%	0.460%	0.478%	0.484%	0.486%
150000	0.134%	0.215%	0.319%	0.310%	0.412%	0.430%	0.436%	0.439%
200000	0.117%	0.192%	0.293%	0.283%	0.383%	0.401%	0.407%	0.410%
400000	0.089%	0.153%	0.242%	0.233%	0.324%	0.342%	0.348%	0.351%

Facility Response RAI SAR 13.3:
Technical Specification 3.7.2(4) shall be removed in a future submittal associated with revisions to the Technical Specifications.

Section 13.2.6 (paragraph 4) of the SAR is revised as follows:

> The Technical Specifications (TS 3.7) include a number of restrictions and requirements to minimize experiment hazards. Experiments containing fissile material (fueled experiments) or explosive material are presently not allowed in the UMLRR core and would require a separate analysis and license amendment.

Facility Response RAI SAR 13.4:
The description of the trip actuator amplifiers (TAAs) in the SAR Section 3.5.3 is provided to illustrate the redundancy associated with the Reactor Protection System (RPS). The description includes the fact that two of the four reactor control blade drive electromagnets are powered by one TAA, and a second identical and independent TAA powers the other two reactor control blade drive electromagnets. The description in Section 3.5.3 is identical to that provided in the SAR of another higher power non-power reactor facility having an identical TAA design.

The SAR Sections 7.1.2 and 7.2.3 summarize the RPS scram circuit operation. The scram circuit is further described in SAR Section 7.4.3, including the redundant and diverse relay and electronic scrams. Most of the circuitry associated with the TAA is designed for initiating the electronic (i.e., fast scram) as described in Section 7.4.3.2. The remainder of the TAA circuitry is relatively simple and is designed for transforming the 120VAC input line voltage to 24VDC power for energizing the electromagnets. The 120VAC input voltage to the TAAs is supplied by two master scram relays connected in series. An open circuit on any of the series wired sensor scram relays or switches (see SAR Table 7-5) will de-energize the master scram relays and consequently interrupt the 120VAC input power to both TAAs.

The electronic scram circuitry is redundant within each TAA. Due to the circuit redundancy, it is highly improbable a malfunction of a TAA could affect the actuation of an electronic scram. Furthermore, as noted in the same SAR section and also in SAR 13.2.2.1, the accident analysis for a rapid reactivity addition and ramp reactivity addition uses the more conservative scram time associated with the slower relay scram. The relay scram is described in SAR 7.4.3.1. Because the relay scram interrupts the 120VAC input line voltage to each TAA, the 24VDC supply from the TAA to the electromagnets is subsequently lost. As a result, a malfunction in a TAA cannot affect the relay scram and subsequent interruption of the 24DC power to the electromagnets.

SAR-14

Facility Response:
Bases for Section 5 of the Technical Specifications shall be included in an upcoming submittal associated with revisions to the Technical Specifications.

END